Unlocking Complexity Using the ECA

Francisco Mesa,
Raúl Rodríguez-Berral, and
Francisco Medina

In the study of electromagnetic wave propagation and scattering, researchers have always faced the dichotomy of dealing directly with Maxwell's equations (and their complicated analytical/numerical solution methods) or trying to find a simplified model (usually in terms of an equivalent circuit) that can help provide some physical insight into the involved electromagnetic phenomena. The pursuit of analytical solutions for propagation, radiation, and scattering problems does not seem to be a task currently in much demand in microwave engineering, although it was only 20 years ago that many research papers on these topics included some sort of analytic derivations.

A Brief History of Equivalent Circuit Models

The impressive progress of computer hardware as well as of computational electromagnetics has rendered most electromagnetic problems, whether simple or very complex, solvable by means of commercial simulators. This trend has the advantage of enabling many different complex electromagnetic scenarios to be analyzed by means of computational resources most research laboratories can afford. However, it has also brought the unfortunate loss of some fruitful skills, among them the ability to find appropriate minimal-order models for complex electromagnetic problems, the relevant parameters of which can be obtained in closed form.

A particular type of problem that exploits the advantages of a minimal-order model approach is the scattering of electromagnetic waves by discontinuities in waveguiding systems. This

Francisco Mesa (mesa@us.es) and Raúl Rodríguez-Berral (rrberral@us.es) are with the Microwaves Group, Department of Applied Physics 1, Escuela Técnica Superior de Ingeniería Informática, Universidad de Sevilla, Spain. Francisco Medina (medina@us.es) is with the Microwaves Group, Department of Electronics and Electromagnetism, Faculty of Physics, Universidad de Sevilla, Spain.

problem was basically dealt with during the first years of microwave engineering development in the 1940s and 1950s; relevant contributors were, among others, J. Schwinger [1], J.W. Miles [2], G.G. Macfarlane [3], C.G. Montgomery [4], N. Marcuvitz [5], J. Brown [6], L.B. Felsen, and A.A. Oliner [7]. For the problems under consideration, it was generally assumed that only the fundamental mode is propagative along the waveguide and that the infinite set of high-order modes excited by the discontinuity are evanescent. This gave rise to the so-called equivalent circuit approach (ECA), wherein the propagations along the homogeneous waveguide systems are modeled by simple transmission lines (TLs) with their corresponding wave impedances and propagation constants, while the stored energy around zero-thickness discontinuities is modeled as single-shunt lumped admittances (a ⟦ network) is required for finite-thickness discontinuities). This procedure was found to be very fruitful and aided considerably in the development of many waveguide systems.

Although the ECA strategy reviewed in this article has special interest for microwave and antenna engineers working with metallic waveguides and periodic structures, the developed models also find applications in other branches of applied physics.

During the years following these early pioneering works, considerable attention continued to be paid to the topic, extending the ECA to the case of scattering by periodic structures [8]–[21]. The development of frequency-selective surfaces (FSSs) [22] clearly benefited from the ECA, with many applications that have continued into the present [22]–[43]. These scattering problems—a discontinuity inside a waveguide and a periodic array of either metal patches or apertures in a metallic screen—should be considered equivalent. As explained in detail in [44], both are essentially the same mathematical and physical problem: a discontinuity inside a *generalized* waveguide. (Although beyond the scope of the present work, we should mention that similar efforts have been carried out in the synthesis of microwave circuits by means of networks of lumped elements [45], [46].)

It is worth noting that the evolution of the ECA has been determined by the progress of computational electromagnetics. At the outset, most work on the ECA was performed analytically, with an emphasis on obtaining closed-form expressions for all elements of the equivalent network [5]. With advances in efficient numerical computer techniques for analyzing complex discontinuities, the basic idea of having an ECA still remains useful, but the analytical effort has generally been replaced by purely numerical procedures. Using these procedures, the elements of the circuit network are computed a posteriori by means of some fitting numerical method [23], [47], after the electromagnetic behavior of the scattering problem is fully known from a full-wave simulation. This combined technique can be very convenient for certain applications, such as optimization tasks, where simple coarse models are required [47], [48], but the fact that the circuit model is found only after the structure's full-wave electromagnetic behavior is characterized essentially obviates the necessity of the equivalent circuit.

Regardless of the ECA's frame of application, this approach is intrinsically an approximate solution to the actual electromagnetic problem; therefore, it is fundamental to establish its range of validity. Whether the values of the elements are given in closed form or extracted from full-wave simulations, the validity of the approach must be clearly identified and known a priori. In this sense, the ECA is very often applied in the long-wavelength limit [26], [49]–[51]. Within this limit, we find, for instance, that the overall effect of the FSS can be modeled as a homogenized surface with a given closed-form surface impedance/admittance. For frequencies above this long-wavelength limit, many heuristics use information about the location and magnitude of the scattering parameters' maxima and minima to propose a network of lumped elements that exhibits behavior very similar to the original discontinuity.

Because the required information is obtained from a previous full-wave simulation within a given range of frequency and as the elements of this network must be numerically fitted to match the original simulated behavior, the validity range of this approach is clearly limited to the frequencies under consideration. The wider the frequency band of interest, the more involved the numerical procedure and the circuit topology. In contrast with the previously discussed methods, some authors have endeavored to derive both the topology of the equivalent circuit and the values of its elements directly from Maxwell's equations [30], [52]–[54]. Independently, these authors made their derivations following a rationale very similar to the one proposed in the seminal work of N. Marcuvitz [5, pp. 142–145].

Nevertheless, there are some differences and application cases that still make the work of interest:

- the possibility of dealing with a dielectric layered scenario
- the extension of the circuit model around and beyond the onset of the first high-order mode
- simple physical explanations of complex electromagnetic behaviors
- the extension to more than one aperture/patch in the discontinuity
- the possibility of dealing with scatterers of arbitrary planar geometry.

Our aim in this review article is to analyze and discuss all these cases.

Another interesting aspect of the ECA that has received attention in recent years is the straightforward physical interpretation it provides for a number of more or less "exotic" phenomena arising in the field of optics (although some of these have, in fact, been reported at microwave frequencies)—for instance, Wood's anomalies [55], [56]; extraordinary optical transmission (EOT) [57]–[59]; anomalous extraordinary transmission (ET) [60]; ET dips and absorption [61]–[63]; and induced metal transparency [64], [65]. Due to the ECA's ease of use, researchers have been able to provide simple yet satisfactory rationales for such phenomena, which previously were often accounted for by resorting to rather qualitative and sophisticated explanations such as interaction with plasmons [57], spoof plasmons [66], [67], and phase resonances [61], [62]. Thus, Wood's anomalies and ET through two-dimensional (2-D) hole

arrays [28], [54] or one-dimensional (1-D) slit arrays [68]–[70] made in highly conducting screens have been explained with simple but accurate circuit models. Phase resonance phenomena have found an ECA-based explanation in [68] and [71], as has anomalous ET in [29] and [72] and enhanced transparency assisted by coupled periodic structures through opaque solid metal films in [73]. In brief, although the ECA strategy reviewed in this article has special interest for microwave and antenna engineers working with metallic waveguides and periodic structures (e.g., FSSs, artificial magnetic conductors, reflectarrays, or transmitarrays), the developed models also find applications in other branches of applied physics.

Discontinuity in a Generalized Waveguide

The first explanations of so-called EOT through a thick metallic sheet perforated with a periodic array of subwavelength holes [57] (see the comprehensive reviews in [58] and [59]) were linked to the existence of surface plasmons in the perforated screen in optical frequencies (where metals behave like materials with negative permittivity, i.e., like solid plasmas). The experimental evidence of EOT at the millimeter-wave and microwave regimes [74] (in this range metals can be regarded as almost perfect conductors) made it apparent that the existence of genuine plasmons was not key to explaining this phenomenon. It was determined that a very simple equivalent circuit of the aperture discontinuity in the periodic structure's unit cell could account, both qualitatively and quantitatively, for the ET phenomenon [27], [28], in close analogy to the well-known microwave-engineering problem of discontinuity scattering inside a waveguide (the unit cell of the periodic array problem plays the role of a virtual waveguide) [44].

An interesting feature of this ET phenomenon is that it occurs in a region hardly explored by microwave engineers—namely, at frequencies very close to the onset of the diffraction regime (in other words, around the cutoff frequency of the first high-order mode in the virtual waveguide). After this first study of a periodic structure, the same ET phenomenon was also found in an aperture discontinuity inside a metallic circular waveguide [75], which certainly has no periodic equivalent structure and hence no possibility of being explained in terms of any sort of surface waves or plasmons.

By contrast, the equivalent circuit of the discontinuity does behave in a similar way, regardless of the characteristics of the waveguiding system. For that reason, and following the rationale in [44] and [76], in this article, the general problem under consideration will be the scattering of a discontinuity inside what is called a *generalized* waveguide—namely, a waveguide the boundaries of which can be perfect electric walls (PEWs), perfect magnetic walls (PMWs), periodic boundary walls (PBWs), or some combination of the three. Certainly, this general problem includes the usual cases of parallel-plate waveguides (PPWs) and rectangular/circular metallic waveguides, as well as 1-D metal gratings and 2-D FSSs.

In some initial works [28], [75], the equivalent circuit topology was heuristically proposed, and the circuit parameter values were extracted from a few full-wave simulations and further curve-fitting procedures. After these initial contacts with the ECA, our work focused on a more rigorous way of obtaining both the topology of the equivalent circuit and the value of its elements. First steps in this direction were reported in [30] and [32]. More complete and efficient wide-band analytical solutions to these problems were ultimately reported in [52] for 1-D structures, and [54] reported a multimodal version for 2-D structures. The case study of this last work is the scattering problem shown in Figure 1—namely, the scattering of a plane wave

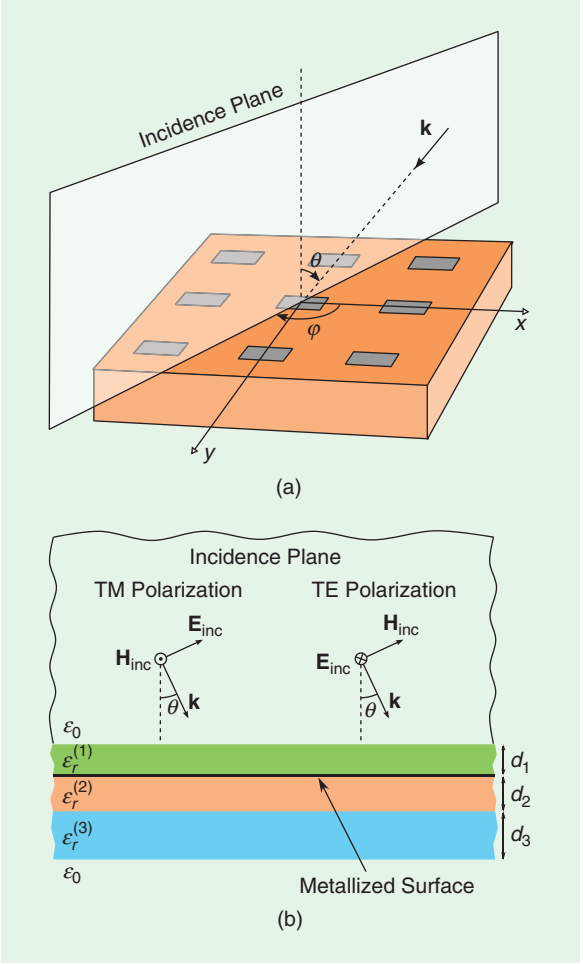

Figure 1. *The structure under study in [54]: the 2-D periodic distribution of rectangular scatterers (metallic patches or apertures in the metallic screen) embedded in a layered dielectric medium. (a) A plane wave impinges obliquely on the structure with its wave-vector orientation characterized by the angles θ and φ. (b) The incidence-plane cut showing the possible transverse electric (TE) and transverse magnetic (TM) polarizations of the incident wave. Each dielectric layer is characterized by its permittivity* $\varepsilon_i = \varepsilon_0 \varepsilon_r^{(i)}$ *and thickness* d_i.

An interesting feature of this ET phenomenon is that it occurs in a region hardly explored by microwave engineers—namely, at frequencies very close to the onset of the diffraction regime (in other words, around the cutoff frequency of the first high-order mode in the virtual waveguide).

impinging on an FSS. Taking into account the periodic nature of this problem, only the unit cell needs to be considered (which is a possible instance of the considered generalized waveguide). The front and side views of this generalized waveguide for the FSS in Figure 1(a) are shown in Figure 2(a) and (b), respectively.

Two Semi-Infinite Media

In this section, we briefly explain the basic analytical derivation carried out in [54], along with the obtained topology and characteristics of the discussed equivalent circuit. A time-harmonic dependence of fields of the type $e^{j\omega t}$ is assumed throughout this work but not explicitly shown. The first and fundamental problem to be considered is the simple discontinuity one shown in Figure 3, which consists of a generalized waveguide with a perforated screen (an iris or a diaphragm) separating two semi-infinite dielectric media.

Taking the waveguide axis along the z direction, the following modal expansion of the electric and magnetic fields at the operation frequency ω can be written at the discontinuity plane ($z = 0$):

$$\mathbf{E}(x,y) = (1+R)\,\mathbf{e}_0(x,y) + \sum_h{}' V_h \mathbf{e}_h(x,y), \tag{1}$$

$$\mathbf{H}^{(1)}(x,y) = Y_0^{(1)}(1-R)[\hat{\mathbf{z}}\times\mathbf{e}_0(x,y)] - \sum_h{}' Y_h^{(1)} V_h [\hat{\mathbf{z}}\times\mathbf{e}_h(x,y)]\,, \tag{2}$$

$$\mathbf{H}^{(2)}(x,y) = Y_0^{(2)}(1+R)[\hat{\mathbf{z}}\times\mathbf{e}_0(x,y)] + \sum_h{}' Y_h^{(2)} V_h [\hat{\mathbf{z}}\times\mathbf{e}_h(x,y)]\,, \tag{3}$$

where subindex $h = 0$ denotes the incident mode, R is the reflection coefficient of the incident wave (this wave has been normalized to have a magnitude equal to 1), V_h stands for the coefficients of the electric field expansion, the superindex (i) refers to the medium ($i = 1, 2$), $Y_h^{(i)}$ is the hth modal admittance in medium (i), and the prime in the summations means that the incident mode is not included in the series of the infinite set of modes.

It should be noted that the reflection coefficient, the V_h coefficients, and the modal admittances are frequency dependent. For 2-D structures, each mode h should be associated with a pair of integer numbers nm. In general, both TM and TE modes are included in the expansion (for 1-D geometries, one of these sets of modes could be excluded if it is not excited by the discontinuity). More details about this expansion and related quantities are given in "Modal Expansion of the Electric and Magnetic Fields."

A key assumption is now made that the transverse electric field at the aperture plane can be written as the following function factorization:

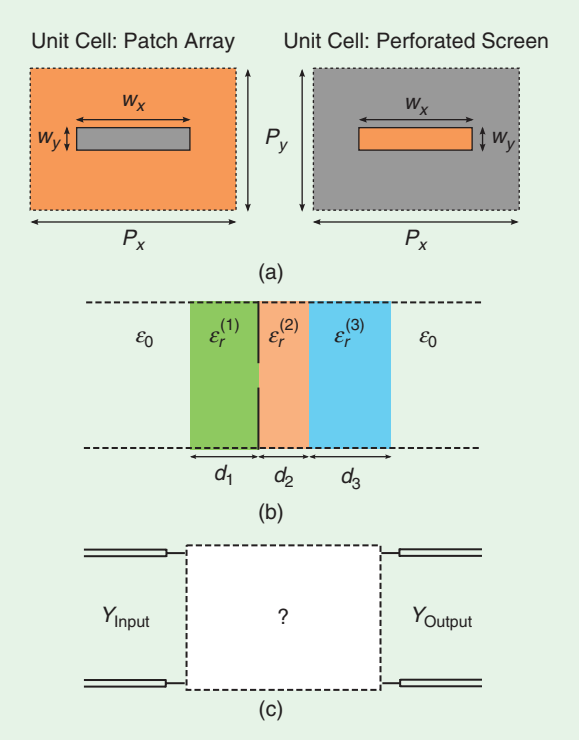

Figure 2. *(a) The front view of the unit cells for the two types of discontinuities considered in this article. The boundaries of the unit cells can be PEWs, PMWs, PBWs, or some combination of the three. (b) A generalized waveguide problem to model the scattering of an incident wave on an aperture discontinuity embedded in a layered medium. (c) Our problem is finding the topology and components of the equivalent network that accounts for the incident wave scattering.*

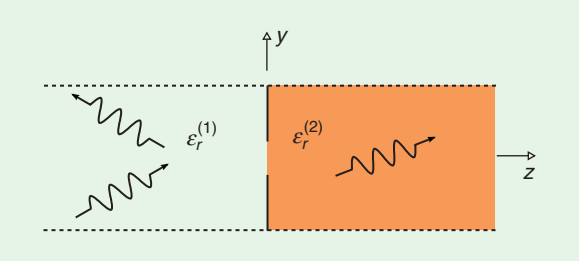

Figure 3. *The fundamental waveguide discontinuity problem associated with a perforated screen located between two homogeneous, semi-infinite media under plane-wave oblique incidence. For purposes of simplicity, the incidence plane is taken as the principal yz plane.*

$$\mathcal{E}_a(x, y; \omega) = G(\omega)\mathbf{E}_a(x, y), \tag{4}$$

where $\mathbf{E}_a(x, y)$ is the considered frequency-independent spatial profile of the electric field at the aperture. Note that this factorization should be considered a reasonable physically based approximation. In a rigorous sense, the frequency and spatial dependences of the aperture field are intertwined (the validity range of this approximation will be discussed in more detail later). Because the aperture field $\mathcal{E}_a$ in (4) must equal the electric field modal expansion in (1) and taking into account that the modes form an orthonormal set, it is straightforward to show (see "Coefficients of the Modal Expansion") that the coefficients of the modal expansion are given by

$$1 + R = G(\omega)\langle \mathbf{e}_0, \mathbf{E}_a \rangle = G(\omega)N_0, \tag{5}$$

$$V_h = G(\omega)\langle \mathbf{e}_h, \mathbf{E}_a \rangle = G(\omega)N_h, \tag{6}$$

In this article, the general problem under consideration will be the scattering of a discontinuity inside what is called a *generalized* waveguide—namely, a waveguide the boundaries of which can be perfect electric walls, perfect magnetic walls, periodic boundary walls, or some combination of the three.

where

$$N_h = \langle \mathbf{e}_h, \mathbf{E}_a \rangle \tag{7}$$

denotes the projection of the assumed aperture field profile onto the hth modal profile. For rectangular waveguide geometries, this projection is directly related to

Modal Expansion of the Electric and Magnetic Fields

The normalized transverse electric field profile, $\mathbf{e}_h(x, y)$, is assumed to be written, in general, as

$$\mathbf{e}_h(x, y) = \hat{\mathbf{e}}_h \cdot \bar{\mathbf{F}}_h(x, y), \tag{S1}$$

where the dyadic $\bar{\mathbf{F}}$ is given in (S2) (see bottom of page) for some particular but practical cases as $[\boldsymbol{\rho} = x\hat{\mathbf{x}} + y\hat{\mathbf{y}}]$.

The periodic boundary wall (PBW) case appears when we deal with two-dimensional (2-D) periodic scatterer arrays (for instance, FSSs). The perfect electric wall (PEW) case corresponds to the instance of rectangular metallic waveguides, and the perfect magnetic wall (PMW) and PEW case (it is assumed that there are PMWs at $x = 0$ and $x = P_x$ and PEWs at $y = 0$ and $y = P_y$) corresponds to the 2-D periodic case under normal incidence, with the incident electric field along the y-direction. Other associated quantities are

$$\mathbf{k}_{t,h} = k_{xn}\hat{\mathbf{x}} + k_{ym}\hat{\mathbf{y}}, \tag{S3}$$

$$= \begin{cases} (k_{x0} + k_n)\hat{\mathbf{x}} + (k_{y0} + k_m)\hat{\mathbf{y}}, & \text{PBW} \\ k_n\hat{\mathbf{x}} + k_m\hat{\mathbf{y}}, & \text{PEW, PMW,} \end{cases} \tag{S4}$$

$$\hat{\mathbf{e}}_h = \begin{cases} \hat{\mathbf{k}}_{t,h}, & \text{TM modes} \\ \hat{\mathbf{k}}_{t,h} \times \hat{\mathbf{z}}, & \text{TE modes,} \end{cases} \tag{S5}$$

$$\hat{\mathbf{k}}_{t,h} = \frac{\mathbf{k}_{t,h}}{|\mathbf{k}_{t,h}|} = \frac{k_{xn}\hat{\mathbf{x}} + k_{ym}\hat{\mathbf{y}}}{\sqrt{k_{xn}^2 + k_{ym}^2}}, \tag{S6}$$

and

$$k_{x0} = k_0 \sin\theta\cos\varphi, \tag{S7}$$

$$k_{y0} = k_0 \sin\theta\sin\varphi, \tag{S8}$$

$$k_n = \frac{\delta\pi n}{P_x}, \tag{S9}$$

$$k_m = \frac{\delta\pi m}{P_y}, \tag{S10}$$

with $\delta = 2$ for PBW and $\delta = 1$ otherwise (k_0 is the vacuum wave number). The modal admittances $Y_h^{(i)}$ are given by

$$Y_h^{(i)} = \frac{H_{t,h}}{E_{t,h}} = \frac{1}{\eta^{(i)}} \begin{cases} k^{(i)}/\beta_{nm}^{(i)}, & \text{TM modes} \\ \beta_{nm}^{(i)}/k^{(i)}, & \text{TE modes,} \end{cases} \tag{S11}$$

with

$$k^{(i)} = \sqrt{\varepsilon_r^{(i)}}\, k_0, \tag{S12}$$

$$\beta_h^{(i)} = \sqrt{\varepsilon_r^{(i)} k_0^2 - |\mathbf{k}_{t,h}|^2}, \tag{S13}$$

$$\eta^{(i)} = \frac{\eta_0}{\sqrt{\varepsilon_r^{(i)}}}, \tag{S14}$$

and η_0 being the free-space impedance.

$$\bar{\mathbf{F}}_h(x, y) = \frac{1}{\sqrt{P_x P_y}} \times \begin{cases} e^{-j\mathbf{k}_{t,h}\cdot\boldsymbol{\rho}}\, \hat{\mathbf{e}}_h\hat{\mathbf{e}}_h, & \text{PBW} \\ \sqrt{2(2 - \delta_{n0})}\cos(k_n x)\sin(k_m y)\,\hat{\mathbf{x}}\hat{\mathbf{x}} + \sqrt{2(2 - \delta_{m0})}\sin(k_n x)\cos(k_m y)\,\hat{\mathbf{y}}\hat{\mathbf{y}}, & \text{PEW} \\ \sin(k_n x)\sin(k_m y)\,\hat{\mathbf{x}}\hat{\mathbf{x}} + \sqrt{(2 - \delta_{n0})(2 - \delta_{m0})}\cos(k_n x)\cos(k_m y)\,\hat{\mathbf{y}}\hat{\mathbf{y}}, & \text{PMW and PEW} \end{cases} \tag{S2}$$

Our problem is finding the topology and components of the equivalent network that accounts for the incident wave scattering.

the Fourier transform of the aperture field profile $\mathbf{E}_a$ (see "Coefficients of the Modal Expansion"). The coefficients of the expansion (1) are then related as follows:

$$\frac{V_h}{N_h} = \frac{1+R}{N_0}. \tag{8}$$

Note that $1+R \equiv V_0$. If every mode h is now associated with a voltage signal V_h, then (8) interprets the N_h projections as transformer turns ratios with the different modes connected, all in parallel, through such transformers.

To complete the derivation of the equivalent network topology, the power continuity (integration of the Poynting vector) through the aperture is imposed:

$$\iint_{\text{ap.}} [\mathbf{E}_a^* \times (\mathbf{H}_2 - \mathbf{H}_1)] \cdot \hat{\mathbf{z}} \, dx dy = 0. \tag{9}$$

This condition will give us the expression for the equivalent network currents consistent with the circuit topology suggested by (8). After introducing (2) and (3) into (9), the following relation is obtained:

$$N_0^* Y_0^{(1)}(1-R) - \sum_h{}' N_h^* Y_h^{(1)} V_h = N_0^* Y_0^{(2)}(1+R) + \sum_h{}' N_h^* Y_h^{(2)} V_h. \tag{10}$$

Now, taking the corresponding modal admittance $Y_h^{(i)}$ in (S11) as the characteristic admittance of a TL associated with the hth mode, the term $\pm Y_h^{(i)} V_h$ can be identified as the current in the hth TL on side (i) (signal propagation along the positive/negative z direction is given by the ± sign), which allows us to rewrite (10) as

$$\sum_h N_h^* I_h^{(1)} = \sum_h N_h^* I_h^{(2)}. \tag{11}$$

This equation, together with (8), has an apparent correspondence with the multimode equivalent network shown in Figure 4(a). In this equivalent network, each TL associated with mode h in medium (i) is connected in parallel to every other TL through its corresponding transformer of ratio N_h.

Basic derivations [78] can be carried out in this equivalent network to find the following scattering parameters corresponding to an input p mode in medium (i) and an output q mode in medium (j) [see Figure 4(b)]:

$$S_{i(p),i(p)} = \frac{|N_p|^2 Y_p^{(i)} - |N_q|^2 Y_q^{(j)} - Y_{\text{eq}}}{|N_p|^2 Y_p^{(i)} + |N_q|^2 Y_q^{(j)} + Y_{\text{eq}}}, \tag{12}$$

Coefficients of the Modal Expansion

The projection of identity $G(\omega)\mathbf{E}_a(x,y) = \mathbf{E}(x,y)$ onto the normalized transverse profile of the sth mode yields

$$G(\omega)\langle \mathbf{e}_s, \mathbf{E}_a \rangle = (1+R)\langle \mathbf{e}_s, \mathbf{e}_0 \rangle + \sum_h V_h \langle \mathbf{e}_s, \mathbf{e}_h \rangle, \tag{S15}$$

where the following notation has been used:

$$\langle \mathbf{f}, \mathbf{g} \rangle = \iint_S \mathbf{f}^*(x,y) \cdot \mathbf{g}(x,y) \, dx dy, \tag{S16}$$

with S representing the cross section of the waveguide. Taking into account that the waveguide modes form an orthonormal set, namely,

$$\langle \mathbf{e}_s, \mathbf{e}_h \rangle = \delta_{sh}, \tag{S17}$$

expression (S15) leads to

$$\begin{aligned} 1 + R &= G(\omega)\langle \mathbf{e}_0, \mathbf{E}_a \rangle \\ V_h &= G(\omega)\langle \mathbf{e}_h, \mathbf{E}_a \rangle. \end{aligned} \tag{S18}$$

Using (S1), these projections can be explicitly written as

$$\langle \mathbf{e}_h, \mathbf{E}_a \rangle = \hat{\mathbf{e}}_h \cdot \iint_{\text{apert}} \overline{\mathbf{F}}_h^*(x,y) \cdot \mathbf{E}_a(x,y) \, dx dy. \tag{S19}$$

For the case of a waveguide with a periodic boundary wall (for instance when the structure under study is a frequency-selective surface), the substitution of (S2) into (S19) leads to

$$\begin{aligned} \langle \mathbf{e}_h, \mathbf{E}_a \rangle &= \frac{1}{\sqrt{P_x P_y}} \hat{\mathbf{e}}_h \cdot \iint_{\text{apert}} \mathbf{E}_a(x,y) \, e^{j\mathbf{k}_{t,h} \cdot \rho} \, dx dy \\ &= \frac{1}{\sqrt{P_x P_y}} \hat{\mathbf{e}}_h \cdot \tilde{\mathbf{E}}_a(\mathbf{k}_{t,h}), \end{aligned} \tag{S20}$$

where $\tilde{\mathbf{E}}_a(\mathbf{k}_{t,h})$ is the standard Fourier transform of function $\mathbf{E}_a(x,y)$. In the cases of a perfect electric wall and/or perfect magnetic wall, a combination of sine and cosine Fourier transforms is obtained for rectangular waveguides.

When the aperture's geometric shape is rectangular, one can propose appropriate aperture field profiles, whose exponential or sine/cosine Fourier transforms are known in closed form. For a generalized waveguide with a canonical geometry other than rectangular, other generalized Fourier transforms will appear (for instance, the Fourier-Bessel transform for circular metallic waveguides).

$$S_{j(q),i(p)} = \frac{2N_q N_p^* Y_p^{(i)}}{|N_p|^2 Y_p^{(i)} + |N_q|^2 Y_q^{(j)} + Y_{eq}}, \quad (13)$$

with Y_{eq} being the sought equivalent admittance of the discontinuity, which can be written for this particular case as

$$Y_{eq} = \sum_h |N_h|^2 [Y_h^{(1)} + Y_h^{(2)}] - |N_p|^2 Y_p^{(i)} - |N_q|^2 Y_q^{(j)}. \quad (14)$$

For the very practical case concerning the reflection coefficient (R) of the input waveguide's dominant mode (denoted as $h = 0$), (12) leads to

$$R = S_{1(0),1(0)} = \frac{|N_0|^2 Y_0^{(1)} - |N_0|^2 Y_0^{(2)} - Y_{eq}}{|N_0|^2 Y_0^{(1)} + |N_0|^2 Y_0^{(2)} + Y_{eq}}. \quad (15)$$

Inclusion of Dielectric Layers

After the derivation of the multimodal network associated with a discontinuity placed between two homogeneous media, the inclusion of a layered dielectric environment is fairly straightforward. Because the different modes in the problem do not couple to one another at the dielectric interfaces, the previous single TL accounting for each mode in each homogeneous semi-infinite medium can now simply be replaced by the corresponding cascade of TL sections, where each

For a generalized waveguide with a canonical geometry other than rectangular, other generalized Fourier transforms will appear (for instance, the Fourier-Bessel transform for circular metallic waveguides).

TL section models the propagation of the mode inside each dielectric layer. This substitution is depicted in Figure 5(a) for the particular configuration of dielectrics shown in Figure 1(b).

In general, the previous single $Y_h^{(1)}$ and $Y_h^{(2)}$ admittances of Figure 4(a) should be replaced by the corresponding input admittances $Y_{in,h}^{(L)}$ and $Y_{in,h}^{(R)}$ to the left/right cascade of dielectrics [see Figure 5(c)]. Thus, the equivalent admittance corresponding to the case shown in Figure 5(a) can be written as

$$Y_{eq}^{(in)} = \sum_h |N_h|^2 [Y_{in,h}^{(L)} + Y_{in,h}^{(R)}] - |N_p|^2 Y_{in,p}^{(L)} - |N_q|^2 Y_{in,q}^{(R)}. \quad (16)$$

The possible existence of a backing electric/magnetic wall at any end of the multilayered structure can readily be accounted for by a short/open circuit termination of the cascade of the TL sections. In this way,

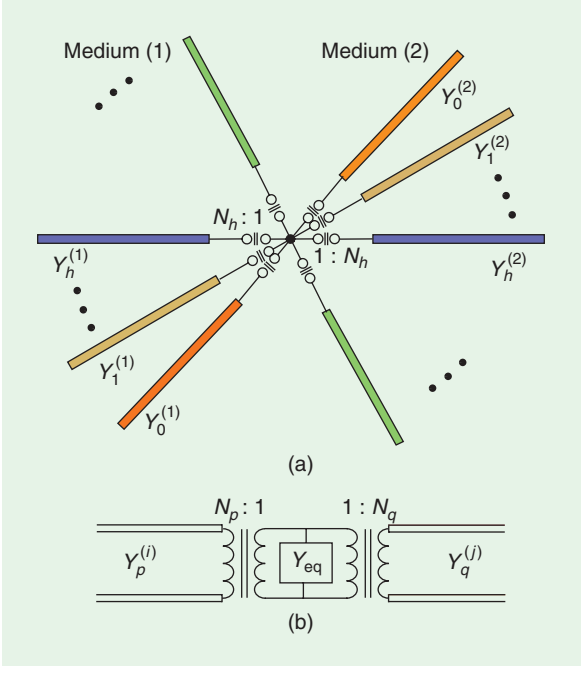

Figure 4. *(a) The top view of the multimodal network representation of the scattering problem associated with a slot-based FSS surrounded by two homogeneous media. Here, the symbol —‖— stands for a transformer. (b) The standard view of the TL problem representing the scattering from the* p*-mode in medium (i) to the* q*-mode in medium (j). The equivalent admittance Y_{eq} accounts for the global effect of the parallel-connected TLs corresponding to all the other modes.*

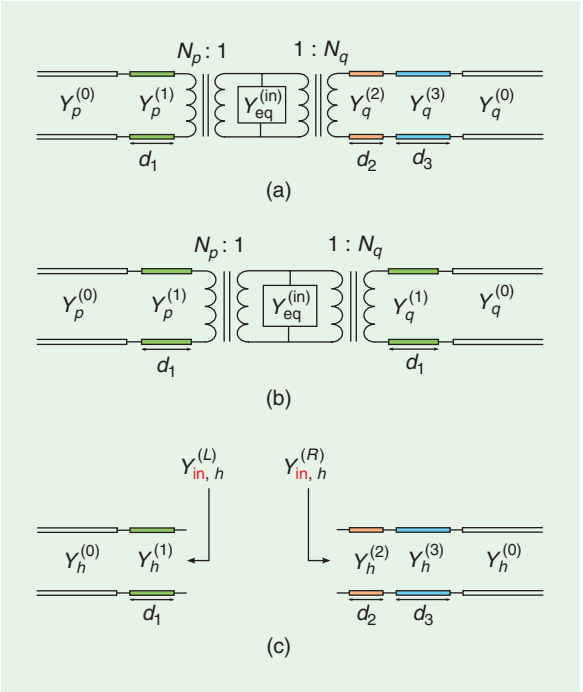

Figure 5. *Considering the multilayered dielectric environment shown in Figures 1(b) and 2(b), this figure shows the equivalent network for computing the scattering parameters corresponding to (a) mode* p *to the left-hand and mode* q *to the right-hand side of the screen and (b) modes* p *and* q *both at the left-hand side of the screen. (c) The definition of the input admittances associated with the hth mode.*

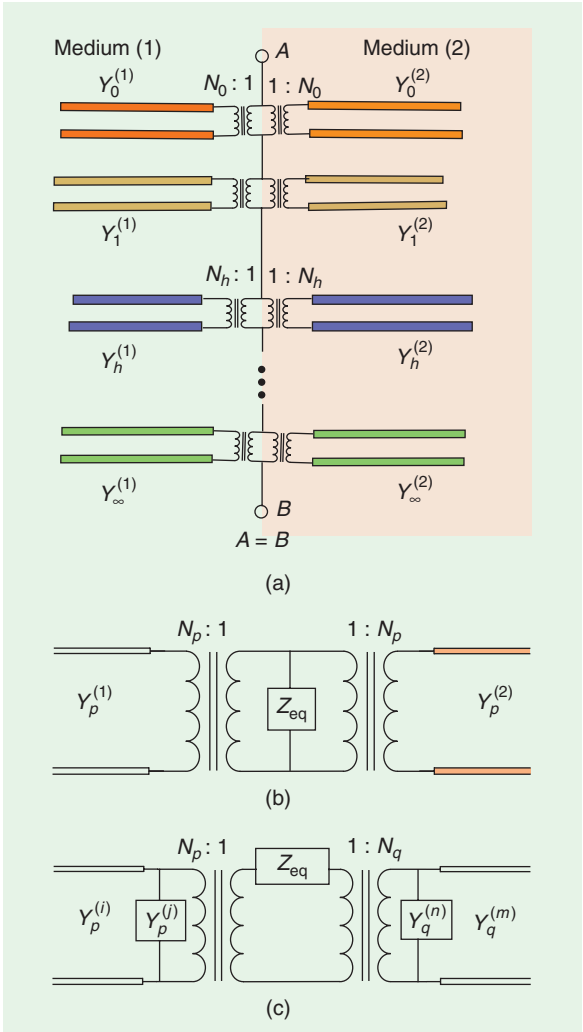

Figure 6. *(a) The multimodal equivalent network associated with a periodic array of metallic scatterers surrounded by two homogeneous media. (b) The equivalent circuit for the scattering of the* pth *order mode. (c) The equivalent circuit for the transmission/reflection from mode* p *in medium (i) to mode* q *in medium (m), with* $p \neq q$, $j \neq i$, *and* $n \neq m$ *(for instance, if* $i = 1$ *and* $m = 2$, *then* $j = 2$ *and* $n = 1$*).*

the existence of actual/virtual electric/magnetic walls along the longitudinal direction in the structure is rigorously introduced in the ECA, regardless of how close or far they might be to the discontinuity.

Patch-Like Discontinuities

The previous sections briefly described the procedure for dealing with aperture-like discontinuities in a generalized waveguide. If the discontinuity consists of a metallic patch (an obstacle-like discontinuity) instead of an aperture, the general procedure is similar although with some differences, as explained in [54]. The main difference is that the problem is now formulated in terms of the surface current density, $J_p(x, y)$, which renders the tangential (transverse-to-z) electric field null at the patch surface. Following [54], the equivalent circuit topology of the discontinuity between two semi-infinite homogeneous media is the one shown in Figure 6, with the transformer ratios given by

$$N_h = \langle \mathbf{J}_p, \mathbf{e}_h \rangle^{-1}. \tag{17}$$

The sought equivalent impedance Z_{eq} appearing in Figure 6(b) and (c) is given by the following series:

$$Z_{eq} = \sum_h{}' \frac{1}{|N_h|^2 (Y_h^{(1)} + Y_h^{(2)})}, \tag{18}$$

where the prime indicates that the sum extends to all the other modes, excluding mode p for the case in Figure 6(b) and both the p and q modes for Figure 6(c). The generalized scattering parameters of this multimodal equivalent network can be obtained by applying the standard procedures of TL theory shown, for instance, in [78].

Other authors have also proposed multimode equivalent networks to deal with similar problems [18], [19], [21], [25]. A distinctive feature of the present proposal is that it takes advantage of the simplified factorization of the field/current in the scatterer to reach an explicit simple topology whose elements are known in closed form.

Further Considerations

Recall that the transformer ratios, N_h, are the only unknown parameters in our ECA. To compute them, we must offer a guess concerning the electric field at the aperture in the discontinuity (or the current density for patch-like discontinuities), as discussed in "Modal Expansion of the Electric and Magnetic Fields."

A first key assumption comes, then, from (4), in that the spatial profile of the aperture electric field remains unchanged in the frequency region of interest. This leads directly to the fact that the transformer ratios given in (7) are independent of frequency (for oblique incidence and PBWs, there would be a very smooth frequency dependence that can be ignored for most practical purposes). Specific closed-form expressions for these coefficients can be found, for instance, by calculating the Fourier transforms of the spatial profiles given in [54, Appendix A].

Thus, the only frequency dependence of the discontinuity's equivalent admittance [see (16)] will come from the input admittances $Y_{in,h}^{(L/R)}$, which are known in closed form. As discussed in [54] and [79], the assumption implicit in (4) is approximately valid up to frequencies close to the scatterer's first excitable high-order resonance. For normal incidence in symmetric FSSs, this resonance would be the scatterer's second even resonance, which is well beyond the onset of the diffraction regime of the structure and, therefore, quite above the usual practical range of interest. In other nonsymmetric situations, the scatterer's first excitable

high-order resonance can appear within the frequency range of interest.

However, in many practical situations, its resonance frequency is high enough to guarantee a wide frequency range of reliable operation for the ECA. Many examples of this wide-band operation have been reported—for instance in [52], [54], and [79].

A second aspect to be considered concerns the apparent need to compute an infinite series for obtaining the equivalent admittance/impedance in (16) and (18) at every frequency of interest. Fortunately, it can easily be proven that the complete series frequency behavior is almost entirely accounted for by just a few dominant terms and that the remaining infinite set (associated with the so-called localized high-order modes [25], [54]) can be expressed as regular frequency-independent inductances and/or capacitances. More details on this decomposition can be found, for instance, in [54, Sec. III].

Example Applications

Now that the topology and different parameters of the equivalent circuit for a generalized waveguide discontinuity embedded in a layered environment have been discussed, along with some relevant computational aspects and limits of validity, in this section we turn to several specific application examples.

1-D Zero-Thickness Metal Strip Gratings

Although the general theory of our ECA was presented in the section "Discontinuity in a Generalized Waveguide" for 2-D structures, it is apparent that 1-D structures can also be treated using the same procedure. A relevant change when dealing with discontinuities in 1-D generalized waveguides is that only the TE/TM modes will be excited by a TE/TM polarized incident wave [52] (this restriction does not apply for conical incidence, i.e., incidence out of the principal planes of the structure). The involved equivalent circuits' topology is clearly simpler as is the complexity of the mathematical procedure (a 1-D series instead of a 2-D series). As an example of application, consider the case shown in Figure 7: the scattering of a TE polarized plane wave by a periodic strip grating printed on a grounded slab.

The TLs to the left and right of Z_{eq} in Figure 7 account for the propagation of the zeroth-order mode (incident and reflected wave) in free space and inside the dielectric, respectively. The short-circuit termination takes into account the presence of the ground plane, and the shunt impedance Z_{eq} represents the global impedance of the equivalent circuit that models the periodic screen, which is given by

$$Z_{\text{eq}} \approx \sum_{n=-N}^{N}{}' \frac{1}{|N_n|^2} \frac{1}{Y_n^{(0)} + Y_{\text{in},n}^{\text{R}}} + j\omega L_{\text{ho}}, \tag{19}$$

where the prime in the sum indicates that the zeroth harmonic is not included, and

In brief, the ECA methodology has been extended, step by step, to provide simple solutions to a variety of periodic structures of interest in the fields of microwave engineering and optics.

$$N_n = \frac{J_0(k_t w/2)}{J_0(k_{t,n} w/2)}, \tag{20}$$

$$Y_{\text{in},n}^{\text{R}} = -jY_n^{(1)} \cot(\beta_n^{(1)} d), \tag{21}$$

where $J_0(\cdot)$ is the Bessel function of the first kind and order zero (following the current profile taken in [52]), $k_{t,n} = k_t + k_n$, $k_t = k_0 \sin\theta$, and $k_n = 2n\pi/P_x$. In the particular cases that $N = 0, 1, 2$ and TE incidence is normal, we find that the corresponding equivalent circuits are those shown in Figure 8, with the L_{ho} inductance given by

$$L_{\text{ho}} = 2\mu_0 \sum_{n=N+1}^{\infty} \frac{J_0^2(k_n w/2)}{k_n[1 + \coth(k_n d)]}. \tag{22}$$

Although the computation of this frequency-independent series can be sped up by means of some acceleration technique, we found that even a brute-force computation of this series is acceptable, given the very reduced central processing unit (CPU) time/effort it requires.

The results for the phase of the reflection coefficient corresponding to equivalent circuits with different values of N are also shown in Figure 8. The considered frequency band ranges over the complete nondiffractive regime, and the 2,000 values of ECA data shown in each plot required no more than 0.5 s on a standard laptop. The ECA data are compared with method of moment (MoM) results obtained using an in-house software that involves a large number of mathematically

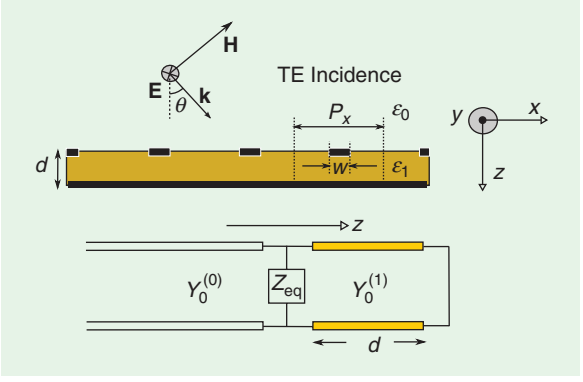

Figure 7. *The equivalent network (bottom) used to model the strip grating (top), printed on a grounded slab under TE polarization illumination. The short-circuit termination accounts for the presence of the ground plane. The shunt impedance Z_{eq} is the global impedance of the equivalent circuit that models the effect of the periodic grating.*

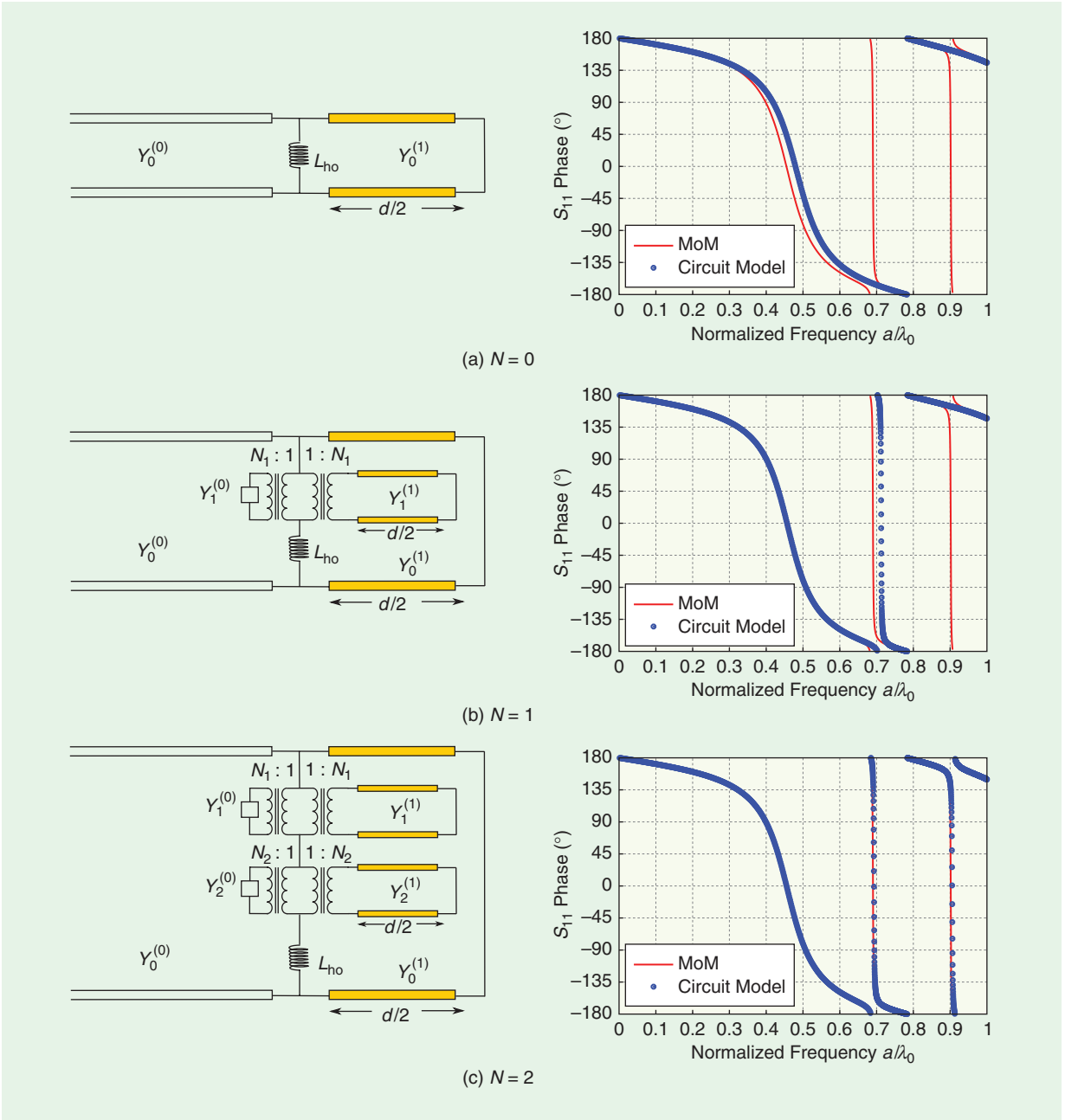

Figure 8. *The left column shows the equivalent networks for the strip grating considered in Figure 7 under normal TE incidence for (a) N = 0, (b) N = 1, and (c) N = 2 (ascending order of complexity and accuracy). The right column shows the phase of the reflection coefficient for (a) N = 0, (b) N = 1, and (c) N = 2, corresponding to the equivalent circuits in the left column. The structure parameters are as follows:* $a \equiv P_x$, $w = 0.1a$, $\varepsilon_r = 10.2$, and $d = 0.2a$.

suitable basis functions (including the correct edge behavior) to achieve a high level of accuracy.

The plot in Figure 8(a) clearly shows that the simplified equivalent circuit with $N = 0$ provides accurate results only for low frequencies. This case would correspond to the long-wavelength limit in which the grating interface has been homogenized and substituted with a purely inductive surface impedance.

The frequency change of the phase and, particularly, the PMW condition (null phase) arises from the compensation of the admittance of L_{ho} by the short-circuit termination translated along the TL section shown in Figure 8(a) (which turns into a capacitive load). However, this condition is not sufficiently well accounted for by this very simple topology, thus requiring the incorporation of additional elements related to high-order modes, as shown by the better agreement found in Figure 8(b). Finally, the relatively simple equivalent circuit corresponding to $N = 2$ in Figure 8(c) is already capable of providing very accurate results in all of the explored wide-frequency band. The models with $N = 1$ and $N = 2$ take into account

the full dynamic interaction of the first high-order modes with the ground plane. Higher-order modes operate far from cutoff, and their contribution is well characterized by L_{ho}. More complex examples involving oblique incidence, TE/TM polarization, and layered environments for 1-D periodic metallic gratings are shown and discussed in [52].

1-D Finite-Thickness Metal Strip Gratings

In this section, we consider the influence of strip thickness on the behavior of a 1-D metal strip grating under TM illumination. The periodic structure under study is shown in Figure 9(a), and its corresponding unit-cell scattering problem in Figure 9(b). To deal with this finite-thickness problem, we will assume that the only relevant mode inside the aperture is the fundamental transverse electromagnetic (TEM) mode, with the effect of the high-order modes only being relevant in the exterior regions. In this way, the equivalent circuit that models the scattering of the finite-thickness discontinuity inside the generalized waveguide shown in Figure 9(b) is given in Figure 9(c), where $C^{(0)}(\omega)$ is just half the capacitance of the aperture surrounded by two identical semi-infinite media (in our case, free space). $Y_0^{(0)}$ stands for the admittance of the TEM mode in a PPW of height p, while $Y_0^{(1)}$ corresponds to the TEM mode of the PPW of height w (the width of the PPW is arbitrary).

The simple network shown in Figure 9(c) can help us understand the results presented in Figure 10, which illustrates the magnitude of the fundamental mode's transmission coefficient for three different values of the strip thickness, t. For the smallest value of t, the TL modeling the inner region is so short that it can be neglected, as shown in Figure 9(d). In this case, we can observe that the transmission coefficient is a function decreasing with frequency, which reaches its minimum at the frequency of the first Wood's anomaly. Wood's anomalies occur at $f_W = nc/P_x \approx 60, 120, \ldots$ GHz, i.e., at the onset of the high-order TM modes where $C^{(0)}(\omega) \to \infty$. Beyond 60 GHz, the diffraction regime starts, and the incident power is distributed in several grating lobes, which prevents the appearance of total transmittance for the considered transmission coefficient.

For the intermediate case $t = 1$ mm, a peak of ET occurs just before the first Wood's anomaly, in close analogy with the case of a 2-D array of subwavelength holes fully discussed in [28]. In this case, it can easily be checked [78] that the TL modeling the propagation of the TEM mode in the electrically short inner region is equivalent to a Π network whose parallel elements are capacitances, and its series element is just an inductance [see Figure 9(e)]. The resulting LC network of the discontinuity thus resonates at a frequency close to the first Wood's anomaly, giving rise to the observed total transmittance. This resonance always happens at some frequency below and close to the Wood's anomaly,

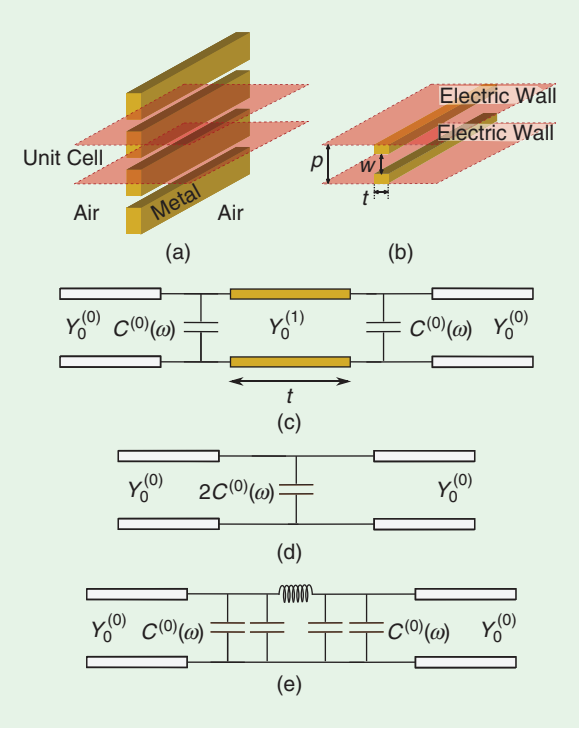

Figure 9. *(a) A 1-D strip grating with finite thickness. (b) A generalized waveguide (unit cell) with a finite-thickness aperture discontinuity. (c) The equivalent network, assuming that the only relevant mode inside the aperture is the fundamental mode. (d) A simplified equivalent network for a negligible electrical thickness. (e) A simplified equivalent network for a small (but nonnegligible) electrical thickness.*

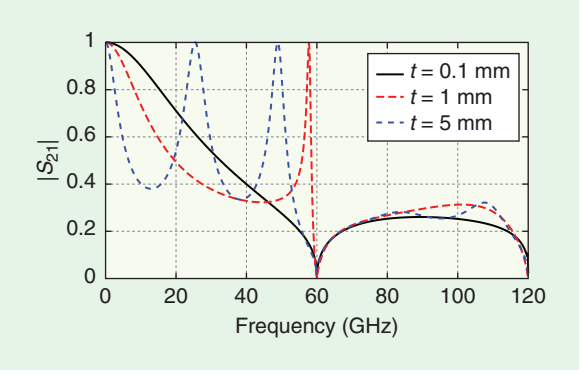

Figure 10. *The magnitude of the transmission coefficient related to a TM plane wave that impinges normally on a metal strip grating with $P_x = 5$ mm, $w = 1$ mm, and different strip thicknesses t.*

where the value of $C_0(\omega)$ approaches infinity. Indeed, this type of resonance should appear for any nonvanishing value of the metal thickness, but it is extremely narrow-band for very thin metal plates.

For the thickest case ($t = P_x$), two transmission maxima appear that can be explained in terms of Fabry-Pérot (FP) resonances inside the thick aperture region. They correspond to the resonances of an electrically

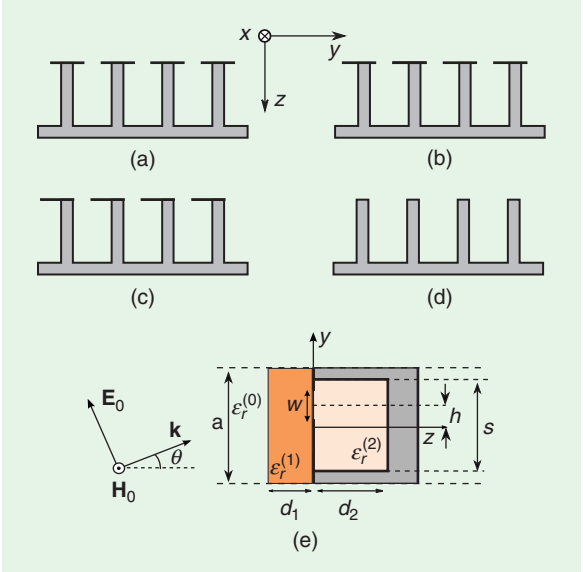

Figure 11. *A cross section of the different types of corrugated planar structures analyzed in the "1-D T-Shaped Corrugated Surfaces" section. (a) A T-shaped corrugated structure with a symmetrically centered slit aperture. (b) A T-shaped corrugated structure with a nonsymmetrical slit position. (c) A T-shaped corrugation with the maximum slit displacement. (d) A classical corrugated surface. All these structures are periodic along the* y *direction and invariant along the* x *direction. (e) The general unit cell including a cover slab and a cavity dielectric filling. The structural parameters are as follows: period* $a \equiv P_y$*; groove size:* s*; slit width:* w*; slit displacement:* h*; external slab thickness:* d_1*; corrugation depth:* d_2*; relative permittivity of the dielectric in the cavity:* $\varepsilon_r^{(2)}$*; relative permittivity in the external slab:* $\varepsilon_r^{(1)}$*; external relative permittivity:* $\varepsilon_r^{(0)}$*; and incidence angle* θ*.*

large TL section of low characteristic impedance terminated by two capacitances in parallel with relatively high characteristic impedance TLs [see Figure 9(c)]. The location of these FP peaks is controlled by the metal plate thickness, whereas the ET peak is defined by the period of the structure. Finally, it should be pointed out that an excellent agreement between the ECA results and those provided by HFSS simulation software [81] has been found in all the previous cases.

1-D T-Shaped Corrugated Surfaces

Another type of 1-D periodic structure that has been satisfactorily analyzed by means of the ECA is the 1-D periodic T-shaped corrugated surface considered in [80]. Some examples of these types of structures amenable to being dealt with using the ECA are shown in Figure 11(a)–(d). The general unit cell of any of these structures is shown in Figure 11(e). To analyze the corrugated structures, the presence of a metallic cavity at the right-hand side of the discontinuity should be taken into account. This implies that the fields in this region must be expanded into the appropriate modal set, which now corresponds to a PPW of height s.

As discussed in [80, Sec. II-C], the inclusion of ohmic losses in the cavity walls for these types of structures can be carried out directly under the usual assumption of strong skin effect. The equivalent circuit for the structure with ohmic losses is shown at the top of Figure 12. In the plot of the magnitude of the reflection coefficient shown in Figure 12, it is interesting to note that the level of ohmic losses is found to be high in the neighborhood of certain frequencies where the structure behaves as an artificial magnetic conductor.

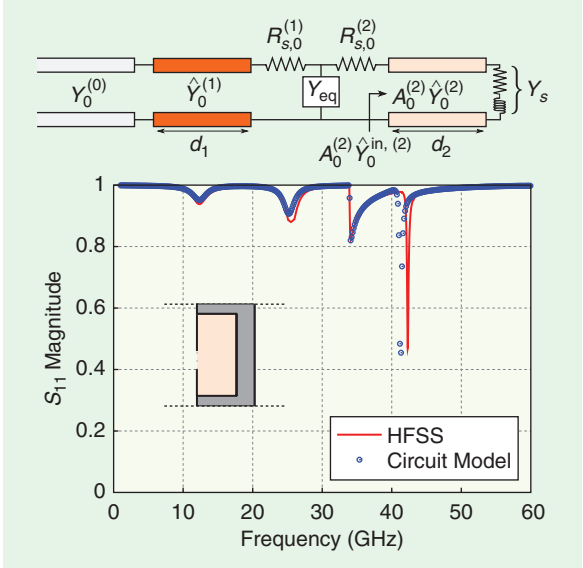

Figure 12. *The magnitude of the reflection coefficient versus frequency. The structure parameters are as follows:* $a = 5$ *mm,* $s = 3$ *mm,* $w = 0.6$ *mm,* $d_1 = 0$*,* $d_2 = 1$ *mm,* $h = 0.6$ *mm,* $\varepsilon_r^{(2)} = 6$*,* $\theta = 50°$*, and* $\sigma_m = 10^6$ *S/m.*

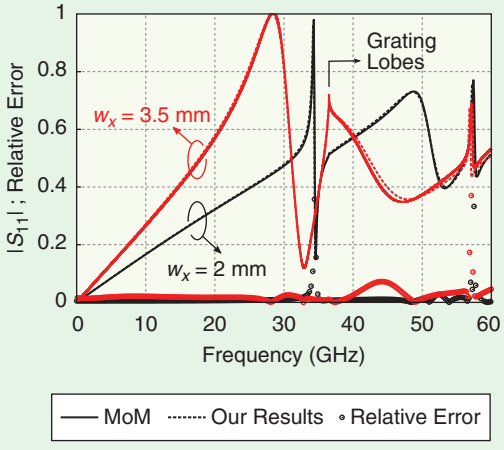

Figure 13. *The magnitude of the reflection coefficient under* $\theta = 40°$ *TE incidence in the* yz *plane* ($\varphi = 90°$) *for the structure in Figure 2(b), with* $\varepsilon_r^{(2)} = 3$*,* $d_1 = 0$*,* $d_2 = 0.5$ *mm,* $d_3 = 0$*,* $P_x = P_y = 5$ *mm, and* $w_y = 0.5$ *mm.*

Around these frequencies, the admittance of the equivalent circuit is purely resistive [80]. For frequencies beyond 34 GHz, we are in the diffraction regime, and the reflection coefficient is not easily interpretable in terms of ohmic losses. However, our ECA data still show a good agreement with the results obtained with HFSS, even in this regime.

2-D Structures with Rectangular Patches/Apertures

When the scatterer causing the discontinuity inside the generalized waveguide under consideration has rectangular geometry, it is easy to obtain closed-form expressions for the transformer ratios in (7) or (17) and, hence, for the elements of the equivalent circuit. According to our discussion in "Coefficients of the Modal Expansion," the assumed spatial profile of the electric field (current density) in the rectangular aperture (patch) discontinuity can be chosen following, for instance, the suggestions in [82]. Because these profiles have a closed-form Fourier transform, analytical expressions can be found for the transformer ratios. A relatively simple computer code will then give us the wide-band frequency behavior of the FSSs, as those studied in [54]; one of these is shown in Figure 13, corresponding to a TE-polarized plane wave that impinges obliquely over an FSS with rectangular metallic patches printed on a dielectric slab.

In the results of Figure 13, it is worth noting the appearance of total reflection at certain frequency values. For the case of $w = 3.5$ mm, this total reflection comes basically from the resonance of each rectangular metallic patch. But the total reflection for the case of $w = 2$ mm is "extraordinary" in nature, similar to the extraordinary total transmission reported in [28] and [57] or the extraordinary reflection reported in [58]; namely, it is directly related to the periodic nature of the structure rather than to the resonance of the scatterers. There is a good agreement with MoM results in a very wide frequency band, even well inside the grating-lobe regime.

An additional example of a structure already studied (in [83]) is shown in Figure 14(c), which plots the magnitude of the transmission coefficient corresponding to a TM-polarized plane wave that impinges obliquely over a periodically perforated metallic screen printed on a silicon substrate. Figure 14(a) illustrates the front and side view of the unit cell of the structure, and Figure 14(b) presents the equivalent circuit employed to compute the ECA results. The circuit model accounts for the

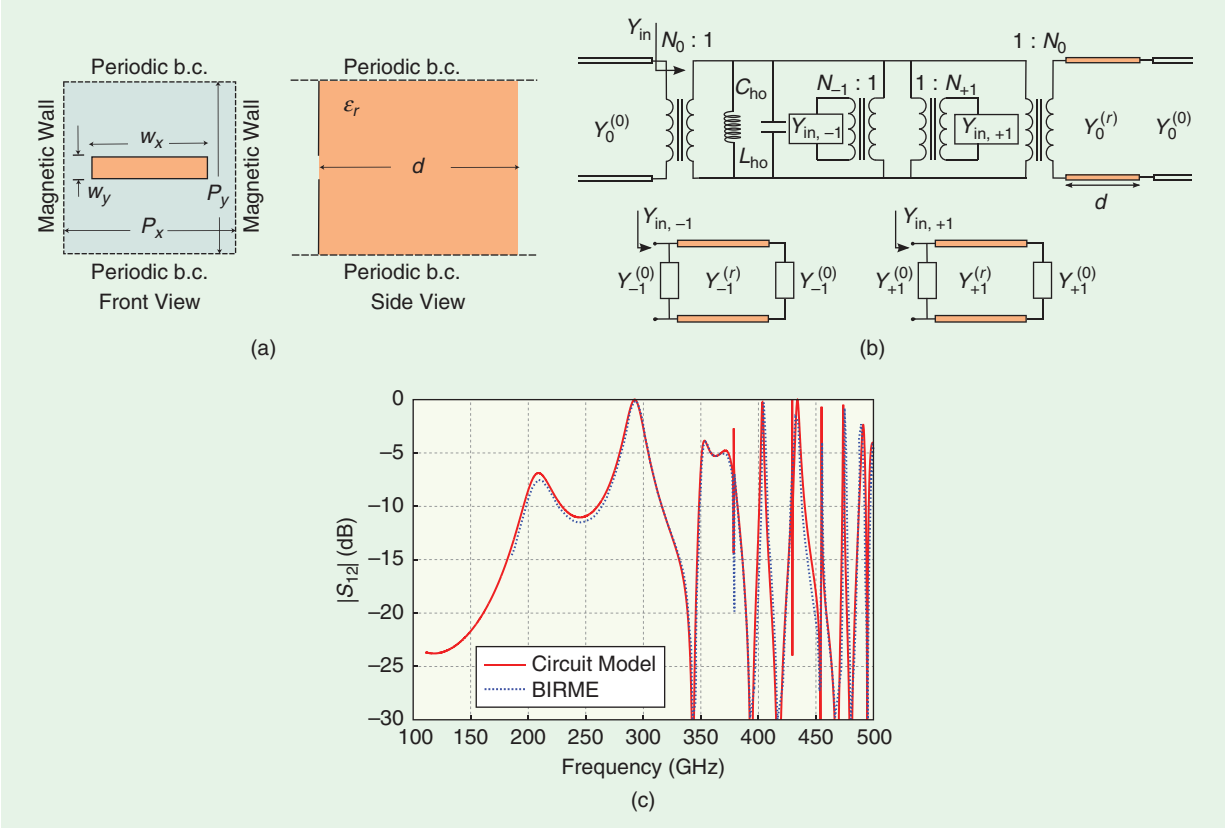

Figure 14. *(a) The front and side views of the periodically perforated metallic screen printed on a silicon substrate previously considered in [83, Figure 4]. (b) The circuit model that takes into account the distributed effects of the first high-order TM modes ($n = 0$, $m = \pm 1$). (c) The magnitude of the transmission coefficient under 20° TM incidence ($\varphi = 90°$). The structural parameters are as follows: $\varepsilon_r^{(2)} = 11.8$, $d_1 = 0$, $d_2 = 302$ μm, $d_3 = 0$, $P_x = P_y = 236$ μm, $w_x = 183$ μm, and $w_y = 30$ μm. The full-wave results in [83] are here denoted as "BIRME." The circuit model results have been obtained using $M = 1$ for both the TE and TM modes. b.c.: boundary conditions.*

Explicit Expressions for Figure 14(b)

The transformers and high-order capacitance and inductance of the equivalent circuit in Figure 14(b) have the following explicit expressions:

$$N_m = 2J_0(\pi/2)\,\mathrm{sinc}\left[(k_0\sin\theta + k_m)\frac{w_y}{2}\right], \quad m = -1, 0, 1; \tag{S21}$$

$$C_{ho} = 4\varepsilon_0 \sum_{n=1}^{\infty}\sum_{m=1}^{\infty} \frac{k_m^2}{k_{nm}^3} F_{nm}^2 \times\left[1 + \varepsilon_r \frac{1 + \varepsilon_r \tanh(k_{nm}d)}{\varepsilon_r + \tanh(k_{nm}d)}(1 - \delta_{m1})\right]; \tag{S22}$$

$$\frac{1}{L_{ho}} = \frac{8}{\mu_0}\sum_{n=1}^{\infty}\sum_{m=1}^{\infty} \frac{k_n^2}{k_{nm}} F_{nm}^2, \tag{S23}$$

where $J_0(\cdot)$ is the Bessel function of the first kind and order zero, $\mathrm{sinc}(\cdot) = \sin(\cdot)/(\cdot)$; and

$$k_n = \frac{2\pi n}{P_x}, \quad k_m = \frac{2\pi m}{P_y}, \quad k_{nm} = \sqrt{k_n^2 + k_m^2}, \tag{S24}$$

$$F_{nm} = \left[J_0\left(\left|k_n\frac{w_x}{2} + \frac{\pi}{2}\right|\right) + J_0\left(\left|k_n\frac{w_x}{2} - \frac{\pi}{2}\right|\right)\right] \times \mathrm{sinc}\left(k_m\frac{w_y}{2}\right). \tag{S25}$$

excitation of high-order TM and TE modes operating well below cutoff through C_{ho} and L_{ho}, respectively. However, the contribution of the first two Floquet harmonics cannot be accounted for by means of such simple circuit components. The distributed nature of the contributions of the $n = 0$ and $m = \pm 1$ harmonics must be explicitly incorporated into the model, as shown in Figure 14(b). Although the equivalent circuit is more complex than a simple LC tank, all the parameters are still known in closed form. [Explicit expressions for the N_0, N_1, and N_{-1} transformers as well as the C_{ho} and L_{ho} elements are given in "Explicit Expressions for Figure 4(b)."] If this enhanced circuit is used, it exhibits a very good agreement between these results and those previously obtained using the highly accurate procedure in [83]. The complex behavior of the transmission coefficient, especially at higher frequencies, is mainly due to many FP resonances in the thick dielectric layer; fortunately, the ECA can account for these resonances in a rigorous way, as shown in the Figure 14.

A final example of a rectangular scatterer is shown in Figure 15, where the magnitude of the transmission coefficient is plotted for the case of a rectangular offset aperture inside a rectangular metallic waveguide. In this example, we show the suitability of the ECA for dealing with discontinuities inside metallic waveguides (in previous examples, only periodic configuration of scatterers were considered—namely, FSSs and/or gratings). We have already dealt with this type of discontinuities in [75]; however, the equivalent circuit presented there was very basic, and the circuit elements were not obtained in closed form but instead using a fitting procedure.

In Figure 15, the ECA-obtained data are compared with results provided by an in-house MoM code, achieving a good agreement within the mono-mode operation band ($f < 2f_{TE_{10}}$). Even beyond this mono-mode operation band, we can observe acceptable agreement that deteriorates only well inside the multimode operation band.

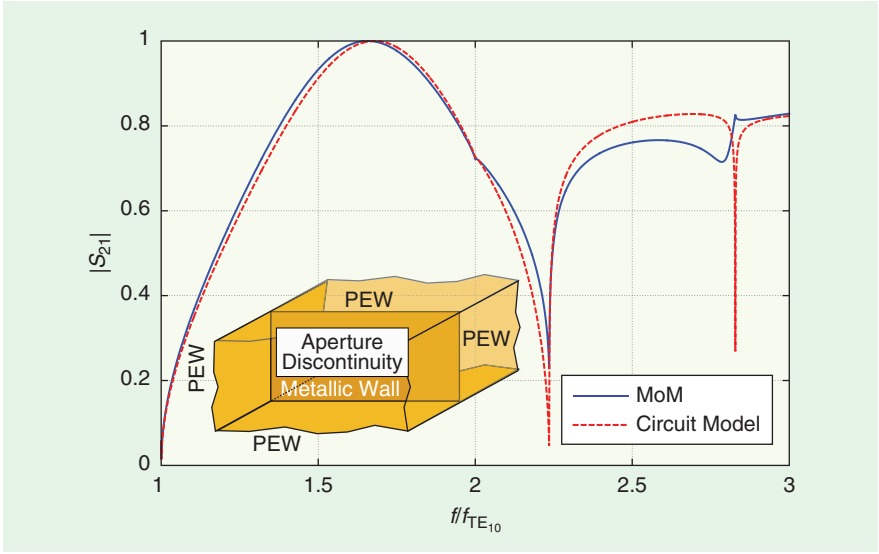

Figure 15. *The magnitude of the transmission coefficient for an aperture discontinuity inside a hollow rectangular metallic waveguide with $a = 2b$; the aperture dimensions are $w_x = 0.6a$, $w_y = 0.15a$; the slit offset is $x_c = y_c = 0.1a$.*

2-D Structures with Arbitrarily Shaped Patches/Apertures

In the previous 2-D examples, the geometry of the considered scatterers was rectangular (in 1-D structures, the present discussion is meaningless), which led us to obtain closed-form expressions for the transformer ratios, assuming that the Fourier transform of the spatial profile was known analytically. The specific shape of the scatterer geometry does not have any influence on the validity of (7); the only relevant consideration concerns the appropriate choice of the spatial profile of the corresponding aperture field (or current density) in the scatterer.

In [84], we proposed employing the spatial profile given by the dominant mode of the hollow-pipe metallic waveguide, the boundary of which coincides with the geometry of the scatterer (if the scatterer

is a metallic patch, we can still employ this procedure [79] to find the current density after invoking the duality principle). The eigen problem to be solved in this case is a purely 2-D problem, for which different efficient numerical solutions are presented in the literature [85], [86]. This required eigenfield can easily be obtained by the eigensolver tool present in most commercial electromagnetic simulators (for instance, using the "solve port only" option in HFSS [81]). Once this spatial profile is obtained numerically, the corresponding Fourier transform can also be obtained numerically by means of an appropriate 2-D implementation of the fast Fourier transform after filtering the data to reduce the numerical noise [79]. It should be noted that, in the present case of arbitrary geometry, closed-form expressions for the circuit elements cannot generally be found.

As an application of the previous procedure, Figure 16 shows the reflection coefficient for a crossed-dipole FSS printed on a dielectric slab. The figure also shows the MoM results provided by Monni et al. in [25, Figure 9] along with data obtained using HFSS. Comparing the ECA results with the other data sets shows that the ECA provides accurate results over a considerably wide frequency band. The overall CPU effort required by the proposed approach is substantially less than that required by other general-purpose full-wave approaches: a few seconds on a typical laptop to cover the considered wide band, as compared to times on the order of minutes for specific-purpose in-house full-wave procedures or hours (or more) for a commercial simulator.

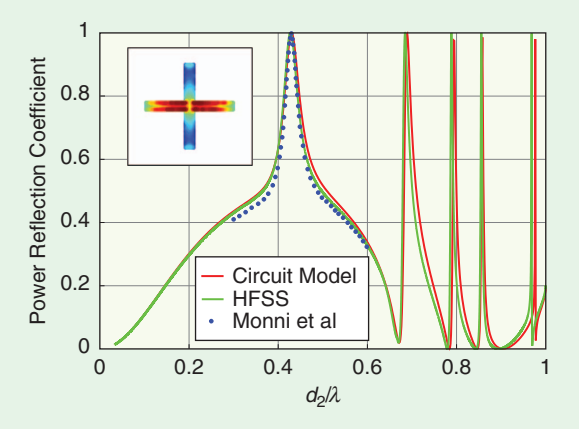

Figure 16. *The power reflection coefficient of a crossed-dipole FSS printed on a dielectric slab with $d_2 = 3$ mm, $\varepsilon_r^{(2)} = 4.0$, and $d_1 = 0$: a comparison with the results reported in [25, Figure 9] and HFSS [81] ($P_x = P_y = 10$ mm). The dimension of the metallic crossed dipole is given in [25, Figure 9]. The inset shows the numerical current pattern.*

Stacked Structures

In this section, we describe how to apply the previous ECA to study a set of consecutive aperture discontinuities along the longitudinal direction of the generalized waveguide; a possible example is the stacked FSS configuration shown in Figure 17.

Before dealing with the stacked structure, we will consider the simpler case of a pair of coupled aperture discontinuities in the generalized waveguide. In particular, we will consider the unit cell with periodic boundary conditions shown in Figure 18, which corresponds to the structure in Figure 17. To study this problem, we can use the even/odd excitation theory [78] so that the analysis of the original coupled structure is reduced to the combined analyses of a single FSS backed by either an electric wall (odd excitation) or a magnetic wall (even excitation). This correspondence is shown in Figure 18 by means of a TL for the fundamental propagating mode in the external region [here denoted as "(0)"] loaded with the corresponding equivalent admittance. This admittance stands for the input admittance of the FSS printed on a dielectric slab of thickness $d_1/2$ terminated with either a magnetic (open-circuit, Y_{eq}^{e}) or an electric (short-circuit, Y_{eq}^{o}) wall (the superscripts "e" and "o" denote even and odd excitations, respectively). Following [87] and [88], Y_{eq}^{e} and Y_{eq}^{o} can be expressed as the following series:

$$Y_{eq}^{(e)} = \sum_{h=1}^{\infty} |N_h|^2 Y_h^{(0)} + j \sum_{h=0}^{\infty} |N_h|^2 Y_h^{(1)} \tan(\beta_h^{(1)} d_1/2), \quad (23)$$

$$Y_{eq}^{(o)} = \sum_{h=1}^{\infty} |N_h|^2 Y_h^{(0)} - j \sum_{h=0}^{\infty} |N_h|^2 Y_h^{(1)} \cot(\beta_h^{(1)} d_1/2), \quad (24)$$

where the index "(1)" refers to the internal dielectric region.

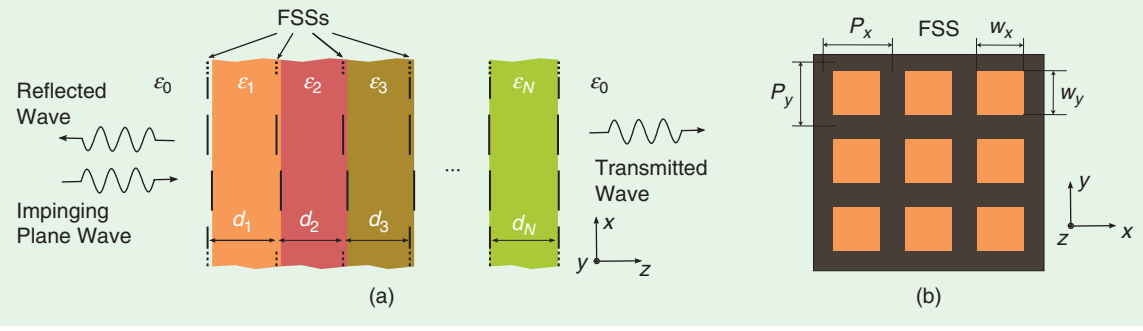

Figure 17. *A schematic representation of a fishnet structure with a finite number of layers: (a) a longitudinal cross section and (b) a front view of the structure.*

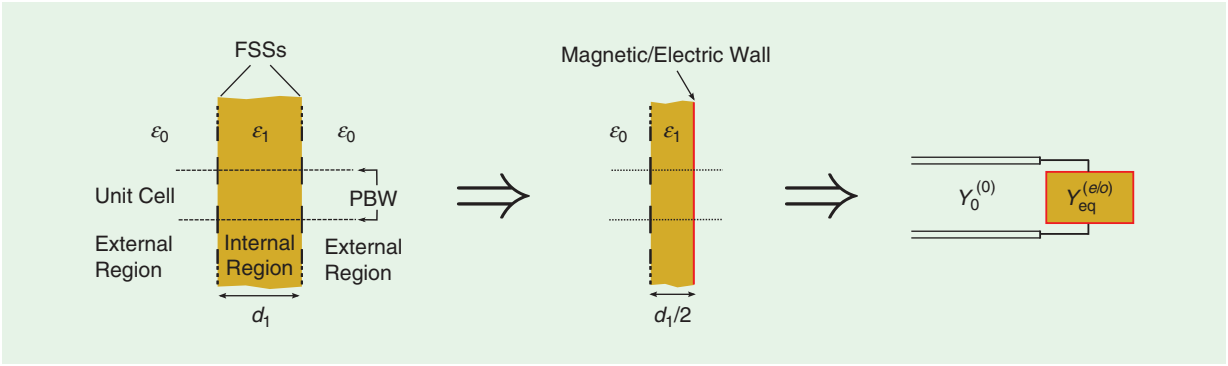

Figure 18. *A pair of coupled FSSs and the associated even/odd excitation (magnetic/electric wall) half-problems with their equivalent circuits.*

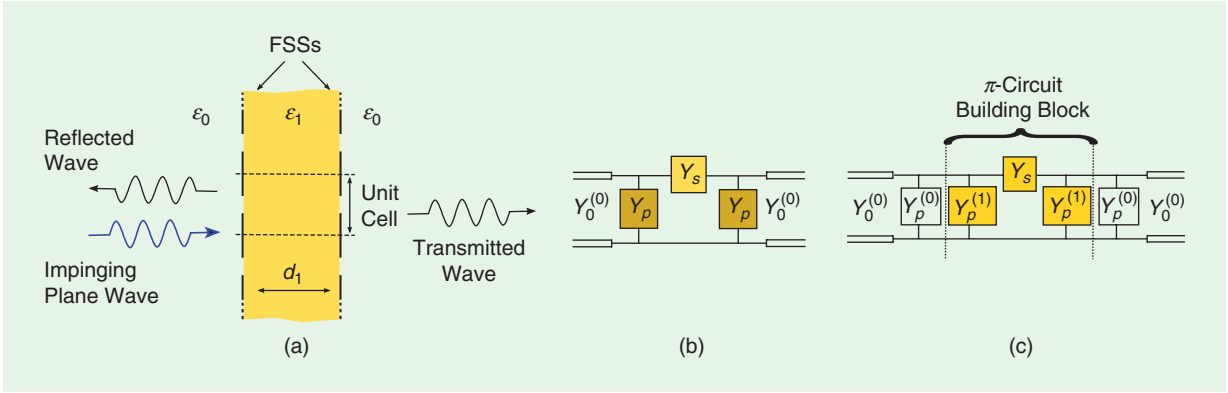

Figure 19. *(a) Two coupled aperture-based FSSs. (b) An equivalent circuit for the scattering of the impinging plane wave in the two coupled FSS structures; the coupled screens are represented by a* Π *network. (c) The equivalent circuit in (b) but showing the decomposition of the parallel element into an external admittance* $Y_p^{(0)}$ *and an internal admittance* $Y_p^{(1)}$.

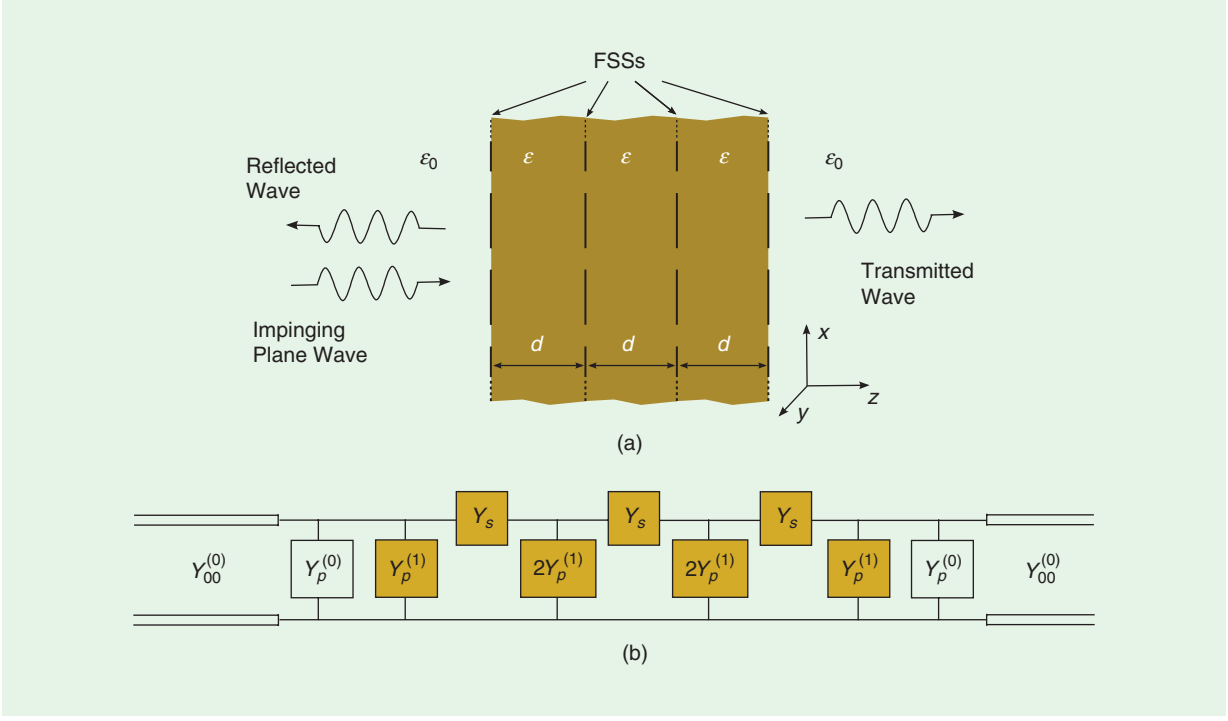

Figure 20. *(a) A stack of four coupled aperture-based FSSs. (b) The equivalent circuit for the scattering of the impinging plane wave in the stacked structure.*

As explained in [88], the key point in finding an appropriate equivalent circuit for the pair of coupled aperture-type discontinuities lies in decomposing the problem into internal and external subproblems. For this purpose, the scattering problem of the original structure in Figure 19(a) can be modeled by means of the equivalent [] network shown in Figure 19(b) or, more importantly, by the internal/external variant given in Figure 19(c). Applying the even/odd excitation theory to the circuit in Figure 19(b), the parallel and series admittances appearing in this [] network can be written in terms of the previous even/odd equivalent admittances in (23) and (24) as

$$Y_{\mathrm{p}} = Y_{\mathrm{eq}}^{(\mathrm{e})}[= Y_{\mathrm{p}}^{(0)} + Y_{\mathrm{p}}^{(1)}], \tag{25}$$

$$Y_{\mathrm{s}} = \frac{1}{2}(Y_{\mathrm{eq}}^{(\mathrm{o})} - Y_{\mathrm{eq}}^{(\mathrm{e})}). \tag{26}$$

From (25) and (26) and the explicit form of (23) and (24), the admittances in Figure 19(c) are given by

$$Y_{\mathrm{p}}^{(0)} = \sum_{h}{}' |N_h|^2 Y_h^{(0)}, \tag{27}$$

$$Y_{\mathrm{p}}^{(1)} = \mathrm{j}\sum_{h} |N_h|^2 Y_h^{(1)} \tan(\beta_h^{(1)} d_1/2), \tag{28}$$

$$Y_{\mathrm{s}} = -\mathrm{j}\sum_{h} |N_h|^2 Y_h^{(1)} \csc(\beta_h^{(1)} d_1). \tag{29}$$

Thanks to the previous decomposition of the pair of coupled aperture-type discontinuities into an internal and an external problem, the stacked structure shown in Figure 20(a) can be modeled by the equivalent network given in Figure 20(b). This procedure can certainly be employed for stacked structures whose internal layers are different, as long as they have the same lattice constants.

As an example of the results obtained with the previous ECA, Figure 21 presents the transmission coefficient of a fishnet structure with five stacked metallic screens. This structure was studied in [87] with the purpose of showing the capabilities of the ECA to study the exotic properties of a class of negative index-medium structures (fishnets) and provide relatively simple explanations for all the observed phenomena. As explained in [87], the results denoted "EC (0,0)" correspond to the simplest topology of the equivalent network and are found to be valid for only low frequencies. More accurate results of the ECA would require a more complex topology, although the relatively simple one corresponding to "EC (1,1)" is already sufficient to model the complex electromagnetic bandgap behavior of this stacked structure.

Other Extensions of the ECA

In all the cases previously examined, the profile of the unknown quantity in the scatterer (aperture field/current density for slot-like/patch-like discontinuities) was assumed to be given by the simple factorization shown in (4). This assumption led to the definition of the transformer ratios given in (7) and (17), as well as

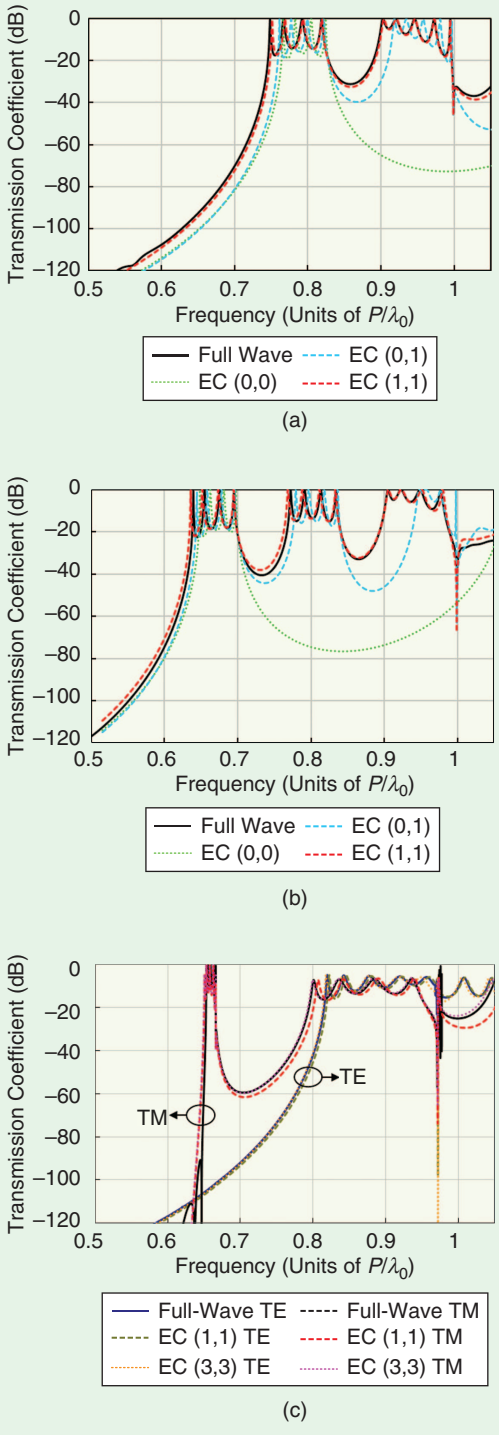

Figure 21. *The transmission coefficient of a finite fishnet structure with $N = 5$ and $P_x = P_y \equiv P$, $w_x = 0.4P$, $w_y = 0.2P$. The equivalent circuit (or "EC") results for (a) $d = 0.6P$ with air and (b) $d = 0.6P$ with dielectric ($\varepsilon_r = 1.4$) between the layers. (c) The oblique incidence ($\theta = 30^o$), with the impinging electric field along the* y *direction for the structure in (a). (c) also shows the equivalent circuit results when a relatively high number of modes is explicitly considered.*

to the application limitations discussed in the "Further Considerations" section. An important extension of the present approach consists of writing the field at the aperture (or the current density in the patch) as the following two-term factorization:

$$\mathcal{E}_a(x, y; \omega) = G_1(\omega)\,\mathbf{E}_{a,1}(x, y) + G_2(\omega)\,\mathbf{E}_{a,2}(x, y). \quad (30)$$

This extension is relevant when dealing with, for instance, compound gratings [61], [62] or multiresonant scatterers, as discussed in [24], [71], and [84].

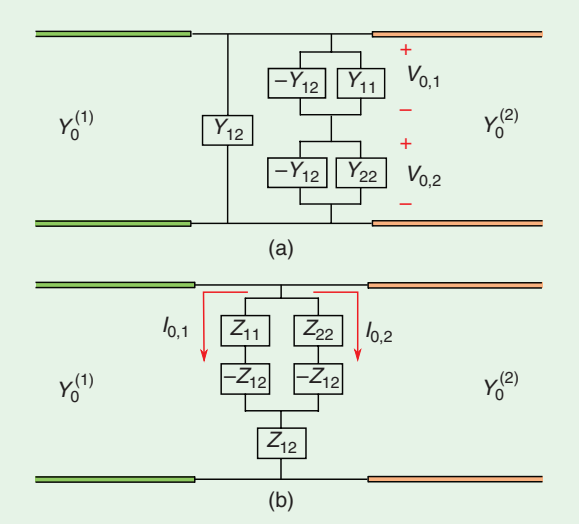

Figure 22. *The equivalent circuit that models the discontinuity formed by (a) apertures and (b) metallic patches. The model takes into account two independent spatial profiles of the unknown quantity in the discontinuity.*

The spatial profiles can be defined either in the same domain, in which case they can model a multiresonant single scatterer, or in different spatial domains, so that compound gratings or several scatterers/apertures per unit cell can be dealt with.

Unfortunately, a basic limitation of this extension turns out to be the impossibility of obtaining multimodal equivalent networks, like the ones shown in Figures 4 and 6. The most we could obtain is the topology for the equivalent admittance of the discontinuity shown in Figure 22, which corresponds to the following expressions (see details of the derivation in [84]):

$$Y_{\text{eq}} = \begin{cases} \left[\dfrac{1}{Y_{11}-Y_{12}} + \dfrac{1}{Y_{22}-Y_{12}}\right]^{-1} + Y_{12}, & \text{apertures} \\ \left(\left[\dfrac{1}{Z_{11}-Z_{12}} + \dfrac{1}{Z_{22}-Z_{12}}\right]^{-1} + Z_{12}\right)^{-1}, & \text{metal patches.} \end{cases} \quad (31)$$

It should be noted that these expressions are obtained provided that $Y_{12} = Y_{21}$. This condition is found when the layout of the unit cell is symmetrical—namely, when each of the spatial profiles in (30) presents a given parity (even or odd). If this condition is not fulfilled, analytical expressions for the shunt discontinuity admittance can be obtained, but such expressions do not have simple correspondent topologies, as those shown in Figure 22.

One relevant application example is illustrated in Figure 23(a), where the results obtained from the equivalent admittance approach for a compound grating with three slits per period are compared with the experimental results provided in [63]. Another example application of the two-term factorization extension corresponds to the 2-D FSS with three dipoles per unit cell in Figure 23(b). The agreement between the ECA results

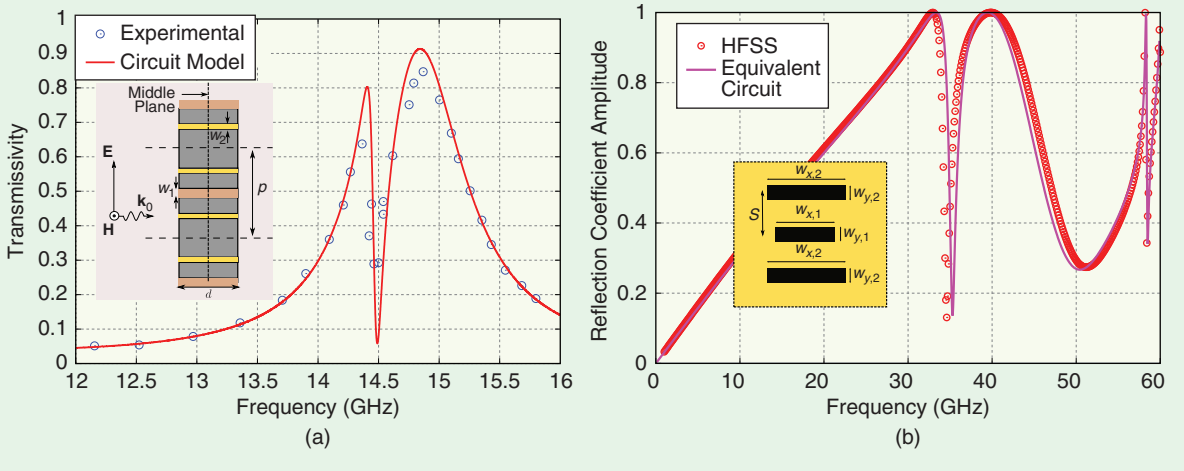

Figure 23. *(a) The transmissivity versus frequency for two different FP bands of the compound grating experimentally studied in [63]. The red solid line corresponds to the analytical results, and the circles are samples of the experimental results in [63]. The structure parameters are as follows: $p = 10$ mm, $w_1 = w_2 = 0.5$ mm, $d_1 = d_2 = 9.9$ mm, $h = 3.375$ mm, $\varepsilon_r^{(1)} = \varepsilon_r^{(2)} = 1$, $\sigma = 3.816{\cdot}10^7$ S/m. (b) The magnitude of the reflection coefficient under normal TM incidence in the xz plane ($\varphi = 0^o$) for an FSS whose unit cell has three dipoles with the following characteristics (distances in mm): $\varepsilon_r^{(2)} = 3.0$, $d_1 = 0$, $d_2 = 0.5$, $d_3 = 0$, $P_x = P_y = 10$; $w_{x,1} = 2.5$, $w_{y,1} = 0.5$, $w_{x,2} = 3.5$, $w_{y,2} = 0.5$; and $s = 1$.*

and those obtained from experiments or numerical HFSS [81] simulations is quite good in both cases.

In addition to the problems and structures considered in this review, the ECA has also been applied to find simple solutions for a variety of problems involving periodic structures as well as to provide alternative simple physical explanations for interesting electromagnetic phenomena. Among these achievements are, for instance, the general case of conical incidence (the incidence plane distinct from the principal optical planes) and polarization conversion, which has been solved in terms of analytically obtained equivalent circuits [54], [84].

In [91], subtle effects associated with metal losses in arrays of extremely narrow slits made in thick metal conductors (see, for instance, [89] and [90]) have been easily explained in terms of conventional lossy TL theory. Arrays of slits with internal structure (steps or smoothly varying geometry) made in thick metal screens, which have been numerically and experimentally studied in the frame of optics and physics journals, have also been modeled using equivalent circuits [92]–[94]. Similarly, this strategy has allowed us to easily analyze structures for multiband absorption [95] or conceived to open transmission bands using opaque grids [96] or generate stopbands using arrays of metal patches [97].

Graphene sheets or patches in stacked configuration have also been amenable to treatment in the frame of the ECA [98], [99]. Microwave transparency through opaque metal thin films induced by coupled arrays of printed strips, recently reported in [65], has been accurately characterized by means of an ECA analytical model [73]. Finally, an ECA model for strongly coupled nonaligned stacked slit arrays has recently been developed [100], [101], thanks to the incorporation of complex transformers with phase-shift response. In brief, the ECA methodology has been extended, step by step, to provide simple solutions to a variety of periodic structures of interest in the fields of microwave engineering and optics.

Conclusions

In this article. we have discussed how to apply the ECA to obtain the topology as well as closed-form (or quasi-closed-form) expressions for the circuit elements of circuit networks associated with planar discontinuities inside a generalized waveguide. The present approach has proven its versatility in dealing with periodic metallic gratings and FSSs embedded in a layered environment and also with discontinuities in metallic waveguides. Apart from the inherent numerical advantage obtained from using analytical procedures, the ECA also provides a very convenient framework to explain many complex and/or exotic electromagnetic phenomena, such as ET through arrays of subwavelength apertures, Wood's anomalies, and electromagnetic-induced transparency. Although the ECA has certain limitations, which we have discussed in this article, its use where appropriate turns the ECA into a very simple, efficient, and fruitful tool for analyzing, designing, and optimizing many microwave devices.

Acknowledgments

We would like to thank Mario Sorolla, Ricardo Marqués, Alexander B. Yakovlev, Jesús M. Rebollar, Jorge Ruíz-Cruz, José R. Montejo-Garai, Miguel Beruete, Víctor Torres, Miguel Navarro-Cía, Carlos Molero, María García-Vigueras, and Diana C. Skigin, among others, for their valuable contributions to the initial development of the present work or their essential participation in later stages of this research. This work has been supported by the Spanish Ministerio de Economía y Competitividad with European Union FEDER funds (project TEC2013-41913-P and project TEC2017-84724-P) and by the Spanish Junta de Andalucía (project P12-TIC-1435).

References

[1] J. Schwinger and D. S. Saxon, *Discontinuities in Waveguides*. New York: Gordon and Breach, 1968.

[2] J. W. Miles, "The equivalent circuit for a plane discontinuity in a cylindrical wave guide," *Proc. IRE*, vol. 34, no. 10, pp. 728–742, Oct. 1946.

[3] G. G. Macfarlane, "Quasi-stationary field theory and its application to diaphragms and junctions in transmission lines and wave guides," *J. Inst. Elec. Eng. 3A*, vol. 93, no. 4, pp. 703–719, Apr. 1946.

[4] C. G. Montgomery, R. H. Dicke, and E. M. Purcell, *Principles of Microwave Circuits* (vol. 8, MIT Radiation Laboratory Series). New York: McGraw-Hill, 1948.

[5] N. Marcuvitz, *Waveguide Handbook* (vol. 10, MIT Radiation Laboratory Series). New York: McGraw-Hill, 1951.

[6] J. Brown, "Artificial dielectrics having refractive indices less than unity," *Proc. IEEE IV-Inst. Monographs*, vol. 100, no. 62R, pp. 51–62, Oct. 1953.

[7] L. B. Felsen and A. A. Oliner, "Determination of equivalent circuit parameters for dissipative microwave structures," *Proc. IRE*, vol. 42, no. 2, pp. 477–483, Feb. 1954.

[8] G. V. Trentini, "Partially reflecting sheet arrays," *IRE Trans. Antennas Propagat.*, vol. 4, no. 4, pp. 666–671, 1956.

[9] R. Ulrich, "Far-infrared properties of metallic mesh and its complementary structure," *Infrared Phys.*, vol. 7, no. 1, pp. 37–55, 1967.

[10] R. Ulrich, "Effective low-pass filters for far infrared frequencies," *Infrared Phys.*, vol. 7, no. 2, pp. 65–74, 1967.

[11] A. Wexler, "Solution of waveguide discontinuitites by modal analysis," *IEEE Trans. Microwave Theory Tech.*, vol. MTT–15, no. 9, pp. 508–517, Sept. 1967.

[12] I. Palocz and A. A. Oliner, "Equivalent network of a multimode planar grating," *IEEE Trans. Microwave Theory Tech.*, vol. 18, pp. 244–252, May 1970.

[13] C.-C. Chen, "Diffraction of electromagnetic waves by a conducting screen perforated periodically with circular holes," *IEEE Trans. Microwave Theory Tech.*, vol. 19, no. 5, pp. 475–481, May 1971.

[14] C.-C. Chen, "Transmission of microwave through perforated flat plates of finite thickness," *IEEE Trans. Microwave Theory Tech.*, vol. 21, no. 1, pp. 1–6, Jan. 1973.

[15] S.-W. Lee, G. Zarrillo, and C.-L. Law, "Simple formulas for transmission through periodic metal grids or plates," *IEEE Trans. Antennas Propagat.*, vol. 30, no. 5, pp. 904–909, May 1982.

[16] C. K. Lee and R. J. Langley, "Equivalent-circuit models for frequency-selective surfaces at oblique angles of incidence," *Proc. IEEE*, vol. 132, no. 6, pp. 395–399, Oct. 1985.

[17] G. Zarrillo and K. Aguiar, "Closed-form low frequency solutions for electromagnetic waves through a frequency selective surface," *IEEE Trans. Antennas Propagat.*, vol. 35, no. 12, pp. 1406–1417, Dec. 1987.

[18] M. Guglielmi and A. A. Oliner, "Multimode network description of a planar periodic metal-strip grating at a dielectric interface. Part I: Rigorous network formulations," *IEEE Trans. Microwave Theory Tech.*, vol. 37, no. 3, pp. 535–541, Mar. 1989.

[19] M. Guglielmi and A. A. Oliner, "Multimode network description of a planar periodic metal-strip grating at a dielectric interface. Part II: Small-aperture and small-obstacle solutions," *IEEE Trans. Microwave Theory Tech.*, vol. 37, no. 3, pp. 542–552, Mar. 1989.

[20] P. Callaghan, E. A. Parker, and R. J. Langley, "Influence of supporting dielectric layers on the transmission properties of frequency selective surfaces," *Proc. IEEE H, Microwave Antennas Propagat.*, vol. 138, no. 5, pp. 448–454, May 1991.

[21] G. Conciauro, M. Guglielmi, and R. Sorrentino, Eds., *Advanced Modal Analysis*, New York: Wiley, 1999.

[22] B. Munk, Ed. *Frequency Selective Surfaces: Theory and Design*, New York: Wiley, 2000.

[23] S. Maci, M. Caiazzo, A. Cucini, and M. Casaletti, "A pole-zero matching method for EBG surfaces composed of a dipole FSS printed on a grounded dielectric slab," *IEEE Trans. Antennas Propagat.*, vol. 53, no. 1, pp. 70–81, Jan. 2005.

[24] R. Dubrovka, J. Vazquez, C. Parini, and D. Moore, "Equivalent circuit method for analysis and synthesis of frequency selective surfaces," *Proc. IEEE H, Microwave Antennas Propagat.*, vol. 153, no. 3, pp. 213–220, Mar. 2006.

[25] S. Monni, G. Gerini, A. Neto, and A. G. Tijhuis, "Multi-mode equivalent networks for the design and analysis of frequency selective surfaces," *IEEE Trans. Antennas Propagat.*, vol. 55, no. 10, pp. 2824–2835, Oct. 2007.

[26] O. Luukkonen, C. Simovski, G. Granet, G. Goussetis, D. Lioubtchenko, A. V. Räisänen, and S. A. Tretyakov, "Simple and accurate analytical model of planar grids and high-impedance surfaces comprising metal strips or patches," *IEEE Trans. Antennas Propagat.*, vol. 56, no. 6, pp. 1624–1632, June 2008.

[27] F. Medina, F. Mesa, and M. Sorolla, "Extraordinary transmission through periodically perforated screens from a circuit theory perspective," in *Proc. Progress Electromagnetics Research Symp.*, Hanghzou, China, 2008, p. 385.

[28] F. Medina, F. Mesa, and R. Marqués, "Extraordinary transmission through arrays of electrically small holes from a circuit theory perspective," *IEEE Trans. Microwave Theory Tech.*, vol. 56, no. 12, pp. 3108–3120, Dec. 2008.

[29] M. Beruete, M. Navarro-Cía, and M. Sorolla, "Understanding anomalous extraordinary transmission from equivalent circuit and grounded slab concepts," *IEEE Trans. Microwave Theory Tech.*, vol. 59, no. 9, pp. 2180–2188, Sept. 2011.

[30] R. Rodriguez-Berral, F. Medina, F. Mesa, and M. Garcia-Vigueras, "Quasi-analytical modeling of transmission/reflection in strip/slit gratings loaded with dielectric slabs," *IEEE Trans. Microwave Theory Tech.*, vol. 60, no. 3, pp. 405–418, Mar. 2012.

[31] F. Costa, A. Monorchio, and G. Manara, "Efficient analysis of frequency-selective surfaces by a simple equivalent-circuit model," *IEEE Antennas Propagat. Mag.*, vol. 54, no. 4, pp. 35–48, Aug. 2012.

[32] M. García-Vigueras, F. Mesa, F. Medina, R. Rodríguez-Berral, and J. L. Gómez-Tornero, "Simplified circuit model for metallic arrays of patches sandwiched between dielectric slabs under arbitrary incidence," *IEEE Trans. Antennas Propagat.*, vol. 60, no. 10, pp. 4637–4649, Oct. 2012.

[33] F. Capolino, A. Vallecchi, and M. Albani, "Equivalent transmission line model with a lumped X-circuit for a metalayer made of pairs of planar conductors," *IEEE Trans. Antennas Propagat.*, vol. 61, no. 2, pp. 852–861, Feb. 2013.

[34] F. Costa, S. Genovesi, A. Monorchio, and G. Manara, "A circuit-based model for the interpretation of perfect metamaterial absorbers," *IEEE Trans. Antennas Propagat.*, vol. 61, no. 3, pp. 1201–1209, Mar. 2013.

[35] B. Blázquez, N. Llombart, D. Cavallo, A. Freni, and A. Neto, "A rigorous equivalent network for linearly polarized THz absorbers," *IEEE Trans. Antennas Propagat.*, vol. 62, pp. 5077–5088, Oct. 2014.

[36] M. Z. Joozdani, M. K. Amirhosseini, and A. Abdol, "Equivalent circuit model for frequency-selective surfaces embedded within a thick plasma layer," *IEEE Trans. Plasma Sci.*, vol. 43, pp. 3590–3598, Oct. 2015.

[37] S. Ghosh and K. V. Srivastava, "An equivalent circuit model of FSS-based metamaterial absorber using coupled line theory," *IEEE Antennas Wireless Propagat. Lett.*, vol. 14, pp. 511–514, 2015.

[38] T. R. SureshKumar, C. Venkatesh, P. Salil, and B. Subbarao, "Transmission line approach to calculate the shielding effectiveness of an enclosure with double-layer frequency selective surface," *IEEE Trans. Electromagn. Compat.*, vol. 57, pp. 1736–1739, Dec. 2015.

[39] D. S. Wang, P. Zhao, and C. H. Chan, "Design and analysis of a high-selectivity frequency-selective surface at 60 GHz," *IEEE Trans. Microwave Theory Tech.*, vol. 64, pp. 1694–1703, June 2016.

[40] P.-C. Zhao, Z.-Y. Zong, W. Wu, and D.-G. Fang, "A convoluted structure for miniaturized frequency selective surface and its equivalent circuit for optimization design," *IEEE Trans. Antennas Propagat.*, vol. 64, pp. 2963–2970, July 2016.

[41] Z. Shen, J. Wang, and B. Li, "3-D Frequency selective rasorber: Concept, analysis, and design," *IEEE Trans. Microwave Theory Tech.*, vol. 64, pp. 3087–3096, Oct. 2016.

[42] H. Li, C. Yang, Q. Cao, and Y. Wang, "An ultrathin bandpass frequency selective surface with miniaturized element," *IEEE Antennas Wireless Propagat. Lett.*, vol. 16, pp. 341–344, 2017.

[43] M. Z. Joozdani and M. K. Amirhosseini, "Equivalent circuit model for the frequency-selective surface embedded in a layer with constant conductivity," *IEEE Trans. Antennas Propagat.*, vol. 65, pp. 705–712, Feb. 2017.

[44] K. Kurokawa, Ed., *An introduction to the theory of microwave circuits*. San Francisco, CA: Academic, 1969.

[45] T. Mangold and P. Russer, "Full-wave modeling and automatic equivalent-circuit generation of millimeter-wave planar and multilayer structures," *IEEE Trans. Microwave Theory Tech.*, vol. 47, no. 6, pp. 851–858, June 1999.

[46] R. J. Cameron, C. M. Kudsia, and R. R. Mansour, Ed., *Microwave Filters for Communication Systems*. New York: Wiley, 2007.

[47] F. Costa and A. Monorchio, "Closed-form analysis of reflection losses in microstrip reflect array antennas," *IEEE Trans. Antennas Propagat.*, vol. 60, no. 10, pp. 4650–4660, Oct. 2012.

[48] J. W. Bandler, R. M. Radoslaw, M. Biernacki, S. H. Chen, P. A. Grobelny, and R. H. Hemmers, "Space mapping technique for electromagnetic optimization," *IEEE Trans. Microwave Theory Tech.*, vol. 42, no. 12, pp. 2536–2544, Dec. 1994.

[49] S. A. Tretyakov, Ed., *Analytical Modeling in Applied Electromagnetics*. Norwood, MA: Artech House, 2003.

[50] O. Luukkonen, F. Costa, C. R. Simovski, A. Monorchio, and S. A. Tretyakov, "A thin electromagnetic absorber for wide incidence angles and both polarizations," *IEEE Trans. Antennas Propagat.*, vol. 57, no. 10, pp. 3119–3125, Oct. 2009.

[51] C. S. R. Kaipa, A. B. Yakovlev, S. I. Maslovski, and M. G. Silveirinha, "Mushroom-type high-impedance surface with loaded vias: Homogenization model and ultra-thin design," *IEEE Antennas Wireless Propagat. Lett.*, vol. 10, pp. 1503–1506, 2011.

[52] R. Rodríguez-Berral, C. Molero, F. Medina, and F. Mesa, "Analytical wideband model for strip/slit gratings loaded with dielectric slabs," *IEEE Trans. Microwave Theory Tech.*, vol. 60, no. 12, pp. 3908–3918, Dec. 2012.

[53] R. Rodríguez-Berral, F. Mesa, F. Medina, and M. García-Vigueras, "Analytical circuit model for dipole frequency-selective surfaces," in *Proc. Int. Microwave Symp.*, Seattle, WA, June 2013.

[54] R. Rodríguez-Berral, F. Mesa, and F. Medina, "Analytical multimodal network approach for 2-D arrays of planar patches/apertures embedded in a layered medium," *IEEE Trans. Antennas Propagat.*, vol. 63, no. 5, pp. 1969–1984, 2015.

[55] R. W. Wood, "On a remarkable case of uneven distribution of light in a diffraction grating spectrum," *Proc. Phys. Soc. London*, vol. 18, no. 1, pp. 269–275, June 1902.

[56] R. W. Wood, "Anomalous diffraction gratings," *Phys. Rev.*, vol. 48, no. 12, pp. 928–937, 1935.

[57] T. W. Ebbesen, H. J. Lezec, H. F. Ghaemi, T. Thio, and P. A. Wolff, "Extraordinary optical transmission through sub-wavelength hole arrays," *Nature*, vol. 391, pp. 667–669, Feb. 1998.

[58] F. J. García-de-Abajo, "Colloquium: Light scattering by particle and hole arrays," *Rev. Mod. Phys.*, vol. 79, pp. 1267–1290, Oct.–Dec. 2007.

[59] F. J. García-Vidal, L. Martín-Moreno, T. W. Ebbesen, and L. Kuipers, "Light passing through subwavelength apertures," *Rev. Mod. Phys.*, vol. 82, pp. 729–787, Jan.–Mar. 2010.

[60] E. Moreno, L. Martín-Moreno, and F. J. García-Vidal, "Extraordinary optical transmission without plasmons: The s-polarization case," *J. Opt. A Pure Appl. Opt.*, vol. 8, pp. S94–S97, Mar. 2006.

[61] A. N. Fantino, S. I. Grosz, and D. C. Skigin, "Resonant effects in periodic gratings comprising a finite number of grooves in each period," *Phys. Rev. E*, vol. 64, p. 016605, June 2001.

[62] D. C. Skigin and R. A. Depine, "Transmission resonances of metallic compound gratings with subwavelength slits," *Phys. Rev. Lett.*, vol. 95, no. 10, p. 217402, 2005.

[63] A. P. Hibbins, I. R. Hooper, M. I. Lockyear, and J. R. Sambles, "Microwave transmission of a compound metal gratings," *Phys. Rev. Lett.*, vol. 96, no. 21, p. 257402, June 2006.

[64] Z. Song, Q. He, S. Xiao, and L. Zhou, "Making a continuous metal film transparent via scattering cancellations," *Appl. Phys. Lett.*, vol. 101, no. 18, p. 181110, 2012.

[65] J. D. Edmunds, M. J. Lockyear, A. P. Hibbins, J. R. Sambles, and I. J. Youngs, "Resonantly overcoming metal opacity," *Appl. Phys. Lett.*, vol. 102, no. 1, p. 011120, 2013.

[66] J. B. Pendry, L. Martín-Moreno, and F. J. García-Vidal, "Mimicking surface plasmons with structured surfaces," *Science*, vol. 305, pp. 847–848, Aug. 2004.

[67] A. P. Hibbins, B. R. Evans, and J. R. Sambles, "Experimental verification of designer surface plasmons," *Science*, vol. 308, pp. 670–672, Apr. 2005.

[68] F. Medina, F. Mesa, and D. C. Skigin, "Extraordinary transmission through arrays of slits: A circuit theory model," *IEEE Trans. Microwave Theory Tech.*, vol. 58, no. 1, pp. 105–115, Jan. 2010.

[69] A. Khavasi and K. Mehrany, "Circuit model for lamellar metallic gratings in the sub-wavelength regime," *IEEE J. Quantum Electron.*, vol. 47, no. 10, pp. 1330–1335, 2011.

[70] E. Yarmoghaddam, G. K. Shirmanesh, A. Khavasi, and K. Mehrany, "Circuit model for a periodic array of slits with multiple propagating diffracted orders," *IEEE Trans. Antennas Propagat.*, vol. 62, pp. 4041–4048, Aug. 2014.

[71] C. Molero, R. Rodríguez-Berral, F. Mesa, and F. Medina, "Dynamical equivalent circuit for 1-D periodic compound gratings," *IEEE Trans. Microwave Theory Tech.*, vol. 64, pp. 1195–1208, Apr. 2016.

[72] M. Beruete, M. Navarro-Cía, S. A. Kuznetsov, and M. Sorolla, "Circuit approach to the minimal configuration of terahertz anomalous extraordinary transmission," *Appl. Phys. Lett.*, vol. 98, no. 1, p. 014106, 2011.

[73] C. Molero, F. Medina, R. Rodríguez-Berral, and F. Mesa, "Making metals transparent: A circuit model approach," *Opt. Express*, vol. 24, no. 9, pp. 10265–10274, May 2016.

[74] M. Beruete, M. Sorolla, I. Campillo, J. S. Dolado, L. Martín-Moreno, J. Bravo-Abad, and F. J. García-Vidal, "Enhanced millimeter wave transmission through quasioptical subwavelength perforated plates," *IEEE Trans. Antennas Propagat.*, vol. 53, pp. 1897–1903, June 2005.

[75] F. Medina, F. Mesa, J. A. Ruiz-Cruz, J. M. Rebollar, and J. R. Montejo-Garai, "Study of extraordinary transmission in a circular waveguide system," *IEEE Trans. Microwave Theory Tech.*, vol. 58, pp. 1532–1542, June 2010.

[76] J. E. Varela and J. Esteban, "Characterization of waveguides with a combination of conductor and periodic boundary contours: Application to the analysis of bi-periodic structures," *IEEE Trans. Microwave Theory Tech.*, vol. 60, no. 3, pp. 419–430, Mar. 2012.

[77] D. G. Dudley, *Mathematical Foundations for Electromagnetic Theory*. New York: IEEE Press, 1994.

[78] D. M. Pozar, *Microwave Engineering*, 3rd ed. Hoboken, NJ: Wiley, 2005.

[79] F. Mesa, M. García-Vigueras, F. Medina, R. Rodríguez-Berral, and J. R. Mosig, "Circuit-model analysis of frequency selective surfaces with scatterers of arbitrary geometry," *IEEE Antennas Wireless Propagat. Lett.*, vol. 14, pp. 135–138, Jan. 2015.

[80] C. Molero, R. Rodríguez-Berral, F. Mesa, and F. Medina, "Analytical circuit model for 1-D periodic T-shaped corrugated surfaces," *IEEE Trans. Antennas Propagat.*, vol. 62, pp. 794–803, Feb. 2014.

[81] ANSYS High Frequency Structure Simulator (HFSS). [Online]. Available: http://www.ansys.com/Products/Simulation+Technology/Electromagnetics/High-Performance+Electronic+Design/ANSYS+HFSS

[82] S. R. Rengarajan, "Choice of basis functions for accurate characterization of infinite array of microstrip reflectarray elements," *IEEE Antennas Wireless Propagat. Lett.*, vol. 4, pp. 47–50, 2005.

[83] S. Biber, M. Bozzi, O. Günther, L. Perregrini, and L.-P. Schmidt, "Design and testing of frequency-selective surfaces on silicon substrates for submillimeter-wave applications," *IEEE Trans. Antennas Propagat.*, vol. 54, no. 9, pp. 2638–2645, Sept. 2006.

[84] F. Mesa, R. Rodríguez-Berral, M. García-Vigueras, F. Medina, and J. R. Mosig, "Simplified modal expansion to analyze frequency selective surfaces: An equivalent circuit approach," *IEEE Trans. Antennas Propagat.*, vol. 64, pp. 1106–1111, Mar. 2016.

[85] F. A. Fernandez and Y. Lu. *Microwave and Optical Waveguide Analysis by the Finite Element Method*. New York: Wiley, 1996.

[86] N. Don, A. Kirilenko, and A Poyedinchuk, "Mode basis computation for the waveguides of arbitrary cross-section," in *Proc. 15th Int. Conf. Microwave Radar and Wireless Communication*, May 2004, pp. 593–596.

[87] V. Torres, F. Mesa, M. Navarro-Cía, R. Rodríguez-Berral, M. Beruete, and F. Medina, "Accurate circuit modeling of fishnet structures for negative-index-medium applications," *IEEE Trans. Microwave Theory Tech.*, vol. 64, pp. 15–26, Jan. 2016.

[88] C. Molero, R. Rodríguez-Berral, F. Mesa, F. Medina, and A. B. Yakovlev, "Wideband analytical equivalent circuit for 1-D periodic stacked arrays," *Phys. Rev. E*, vol. 93, p. 013306(1–14), Jan. 2016.

[89] Y. Takakura, "Optical resonance in a narrow slit in a thick metallic screen," *Phys. Rev. Lett.*, vol. 86, no. 24, pp. 5601–5603, June 2001.

[90] J. R. Suckling, A. P. Hibbins, M. J. Lockyear, T. W. Preist, J. R. Sambles, and C. R. Lawrence, "Finite conductance governs the resonance transmission of thin metal slits at microwave frequencies," *Phys. Rev. Lett.*, vol. 92, no. 14, pp. 147401, Apr. 2004.

[91] R. Yang, R. Rodríguez-Berral, F. Medina, and Y. Hao, "Analytical model for the transmission of electromagnetic waves through arrays of slits in perfect conductors and lossy metal screens," *J. Appl. Phys.*, vol. 109, p. 103107, May 2011.

[92] F. Medina, G. Bigel, F. Mesa, and R. Rodríguez-Berral, "Analytical modeling of structured 1-D diffraction gratings using a microwave engineering approach," in *Proc. 41st European Microwave Conf.*, Manchester, U.K., 2011, pp. 814–817.

[93] F. Medina, R. Rodríguez-Berral, and F. Mesa, "Circuit model for metallic gratings with tapered and stepped slits," in *Proc. 42nd European Microwave Conf.*, Amsterdam, The Netherlands, 2012, pp. 1225–1228.

[94] C. Molero, R. Rodríguez-Berral, F. Mesa, and F. Medina, "Analytical modeling of non-symmetric and non-uniform compound gratings," in *Proc. 46th European Microwave Conf.*, London, U.K., 2016, pp. 100–103.

[95] Y. R. Padooru, A. B. Yakovlev, C. S. R. Kaipa, F. Medina, and F. Mesa, "Circuit modeling of multi-band high-impedance surface absorbers in the microwave regime," *Phys. Rev. B*, vol. 84, no. 3, p. 035108, July 2011.

[96] C. S. R. Kaipa, A. B. Yakovlev, F. Medina, F. Mesa, C. A. M. Butler, and A. P. Hibbins, "Circuit modeling of the transmissivity of stacked two-dimensional metallic meshes," *Opt. Express*, vol. 18, no. 13, pp. 13309–13320, June 2010.

[97] C. S. R. Kaipa, A. B. Yakovlev, F. Medina, and F. Mesa, "Transmission through stacked 2-D periodic distributions of square conducting patches," *J. Appl. Phys.*, vol. 112, p. 033101, Aug. 2012.

[98] C. S. R. Kaipa, A. B. Yakovlev, G. W. Hanson, Y. R. Padooru, F. Medina, and F. Mesa, "Enhanced transmission with a graphene-dielectric micro-structure at low-terahertz," *Phys. Rev. B*, vol. 85, no. 24, p. 245407, June 2012.

[99] Y. R. Padooru, A. B. Yakovlev, C. S. R. Kaipa, G. W. Hanson, F. Medina, and F. Mesa, "Dual capacitive-inductive nature of periodic graphene patches: Transmission characteristics at low-terahertz frequencies," *Phys. Rev. B*, vol. 87, no. 11, p. 115401, Mar. 2013.

[100] C. Molero, R. Rodríguez-Berral, F. Mesa, and F. Medina, "Wideband equivalent circuit for non-aligned 1-D periodic metal strips coupled gratings," in *Proc. 45th European Microwave Conf.*, Paris, France, 2015, pp. 331–334.

[101] C. Molero, R. Rodríguez-Berral, F. Mesa, and F. Medina, "Wideband analytical equivalent circuit for coupled asymmetrical non-aligned slit arrays," *Phys. Rev. E*, vol. 95, p. 023303, Feb. 2017.